8/1-30-96 JSD

Energy Conversion & Storage Program

1994 Annual Report

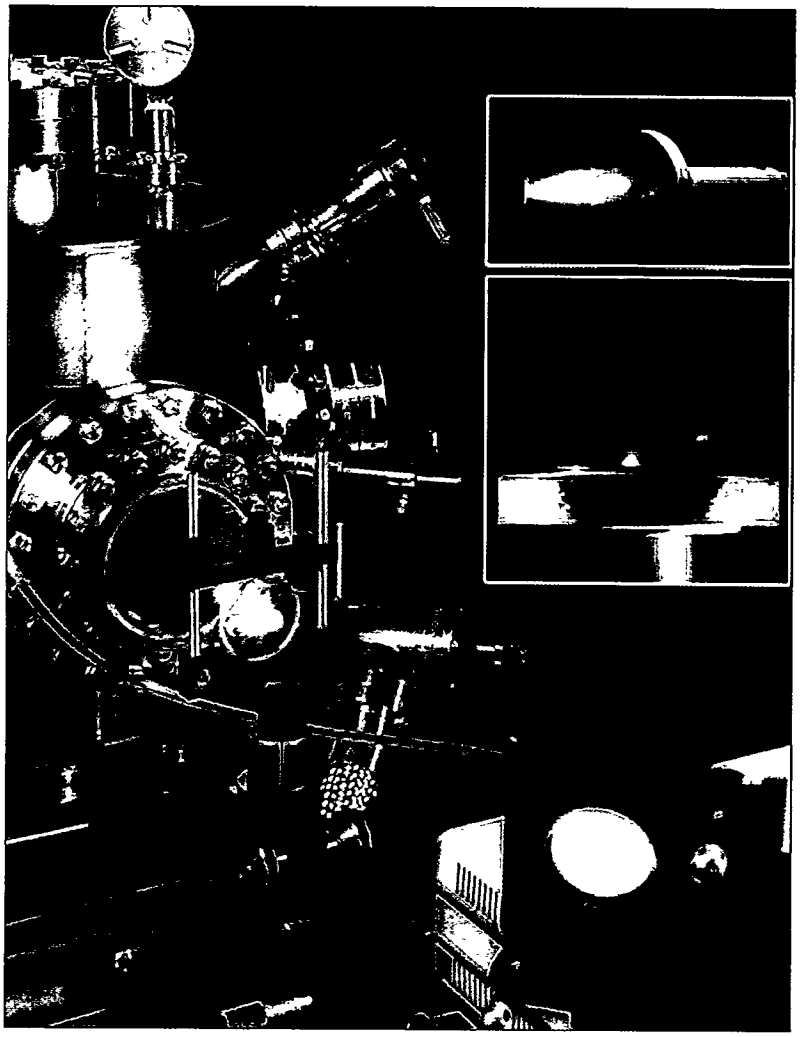

Energy & Environment Division
Lawrence Berkeley Laboratory
UNIVERSITY OF CALIFORNIA

LBL-36552
UC-1400
April 1995

Cover:
New pulsed laser deposition system for fabricating catalyst materials.
Inset: Superconducting target (top) and copper target (bottom).

Available to DOE and DOE Contractors from
Office of Scientific and Technical Information
P.O. Box 62, Oak Ridge, TN 37831
Prices available from (615) 576-8401

Available to the public from
National Technical Information Service
U.S. Department of Commerce
5285 Port Royal Road, Springfield, VA 22161

Prepared for the U.S. Department of Energy under Contract No. DE-AC03-76SF00098

DISCLAIMER

Portions of this document may be illegible in electronic image products. Images are produced from the best available original document.

DISCLAIMER

This report was prepared as an account of work sponsored by an agency of the United States Government. Neither the United States Government nor any agency thereof, nor any of their employees, makes any warranty, express or implied, or assumes any legal liability or responsibility for the accuracy, completeness, or usefulness of any information, apparatus, product, or process disclosed, or represents that its use would not infringe privately owned rights. Reference herein to any specific commercial product, process, or service by trade name, trademark, manufacturer, or otherwise does not necessarily constitute or imply its endorsement, recommendation, or favoring by the United States Government or any agency thereof. The views and opinions of authors expressed herein do not necessarily state or reflect those of the United States Government or any agency thereof.

Energy Conversion & Storage Program 1994 Annual Report

Elton J. Cairns, Program Head

Energy & Environment Division
Lawrence Berkeley Laboratory
University of California
Berkeley, California 94720
(510) 486-5001

Report No. LBL-36552

DISTRIBUTION OF THIS DOCUMENT IS UNLIMITED

MASTER

Contents

Introduction

The Energy Conversion and Storage Program investigates state-of-the-art electrochemistry, chemistry, and materials science technologies for:

- development of high-performance rechargeable batteries and fuel cells;
- development of high-efficiency thermochemical processes for energy conversion;
- characterization of complex chemical processes and chemical species;
- study and application of novel materials for energy conversion and transmission.

Research projects focus on transport-process principles, chemical kinetics, thermodynamics, separation processes, organic and physical chemistry, novel materials, and advanced methods of analysis.

Electrochemistry research aims to develop advanced power systems for electric vehicle and stationary energy storage applications. Applied studies are conducted to elucidate fundamental electrochemical processes. Advanced spectroscopic and traditional electrochemical characterization methods are used to study new electrochemical systems. Topics include the exploratory development of new electrochemical couples for advanced rechargeable batteries, improvements in batteries and fuel-cell materials, the establishment of engineering principles applicable to electrochemical energy storage and conversion, and the characterization of lithium-polymer electrolyte cells for the U.S. Advanced Battery Consortium. The Program is the lead center for management of the Exploratory Technology Research (ETR) program, designed to identify new electrochemical couples for advanced batteries, with major emphasis on applied research that will lead to superior performance and lower life-cycle costs.

Chemical applications research includes topics such as separations, catalysis, fuels, and chemical analyses. Included in this program area are projects to develop improved, energy-efficient methods for processing product and waste streams, coal gasifiers, and biomass conversion processes. The development of reliable new methods for removing solids and gaseous contaminants from coal-gas at high temperature and pressures is one of the most important technological advances required in the field of coal gasification. Reversible chemical complexation is investigated for selective separations of compounds from formation media for product recovery. The use of polymer pendant organic ligands is investigated as an efficient technology for the removal and recovery of toxic metal ions from waste streams. Extended x-ray absorption fine structure (EXAFS) is combined with electrochemical processes to obtain a thorough understanding of the lithium intercalation processes on an atomic level. Laser-material interactions are being investigated for sensitive chemical analyses of environmental and waste-stream species.

Materials applications research includes the evaluation of the properties of advanced materials, as well as the development of novel preparation techniques. Pulsed laser deposition is being used to produce high-temperature superconducting thin films and new rechargeable battery electrode materials. Sol-gel and solvent extraction methods are used to produce aerogel superinsulators; and light-scattering techniques are being adapted to characterize sea water and sea ice in order to better interpret remote observations of the surface of the earth.

Program Staff

Elton J. Cairns, Program Head

Thomas Adler
Michael Ayers
Paul Berdahl
Edério Bidóia
Harvey Blanch
Robert Broekhuis
Mark Brooks
Garth Burns
Manuel Caetano
Van Carey
Jie Chen
Daniel Chinn
Yohan Choi
Xi Chu
Douglas Clark
Christopher Coen
Stephen Cramer
Robert Darling
Charles Deng
Zhongyi Deng
Liliane DeSouza
Joszef Devenyi
Marc Doyle
Laurent Fenouil
Alberto Fernandez
Richard Fish
Dania Ghantous
Melissa Grush
Craig Horne
Song Ping Huang
Arlon Hunt
Mary Quinby-Hunt
Scott Husson
Sungho Jeong
Jordan Kahn
John Kerr
Marvin Kilgo
C. Judson King
Kim Kinoshita
Karen Koigawachi
Fanping Kong
Robert Kostecki
Henry Kuo
Chun-Pong Lau
Susan Lauer
Wei Li
Scott Lynn
Xianglei Mao
Diana Marmorstein
Frank McLarnon
Jeremy Meyers
David Miller
Jeffrey Moore
John Newman
Carolyn Pals
Blaine Paxton
Bavanethan Pillay
Robert Plievelich
Kathryn Podolske
Alain Rabion
Clayton Randall
Lin Rao
Ronald Reade
Paul Ridgway
Diedra Rolland
James Rudnicki
Benjamin Rush
Richard Russo
Robert Selleck
Mark Shannon
Xiangyun Song
Jonathan Spear
Charlotte Standish
Peter Stevens
Kathryn Striebel
Waltraud Taucher
Minmin Tian
Jerome Thomas
Jan van Elp
Hongxin Wang
Xiaodong Wang
Xin Wang
Shi-Jie Wen
Charles Wilkes
Chin-On Wong
Mark Yahnke
Shouquan Zeng

Electrochemistry

Exploratory Technology Research Program for Electrochemical Energy Storage

E.J. Cairns, K. Kinoshita, and F.R. McLarnon

The Lawrence Berkeley Laboratory (LBL) is lead center for management of the Exploratory Technology Research (ETR) Program, which is supported by the Electric/Hybrid Propulsion Division of DOE's Office of Transportation Technologies. This program's research supports DOE development of electrochemical energy conversion systems for potential use in electric vehicles. The most-promising electrochemical technologies are identified and transferred to the U.S Advanced Battery Consortium (USABC) and/or to another DOE program for further development and scale-up.

The ETR Program identifies new electrochemical couples for advanced batteries, determines the technical feasibility of the new couples, improves battery components and materials, establishes engineering principles applicable to electrochemical energy storage and conversion, and investigates fuel cell and metal/air systems for transportation applications. Major emphasis is given to applied research that will lead to superior performance and lower life-cycle costs.

The LBL senior investigators participating in the project are E.J. Cairns, K. Kinoshita, F.R. McLarnon, and J.S. Newman of the Energy and Environment Division; and L.C. DeJonghe, J.W. Evans, P.N. Ross, and C.W. Tobias of the Materials Sciences Division. Research projects conducted by subcontractors are described in the recent annual report, Exploratory Technology Research Program for Electrochemical Energy Storage (LBL-35567); LBL in-house work is summarized in the next article. Highlights of the ETR Program subcontracted work follow.

Exploratory Research

The objectives of a subcontract with the Advanced Energy Systems Division of Acme Electric Corporation are to evaluate the LBL family of ternary electrolytes for extending the cycle life of large-size Zn/NiOOH cells and to develop Zn/NiOOH battery technology for EV applications. Acme Electric Corporation has completed 175 charge/discharge cycles with a 20-Ah starved-electrolyte Zn/NiOOH cell that contains a low-alkaline electrolyte developed at LBL.

Oak Ridge National Laboratory (ORNL) has fabricated all-solid-state Li/$Li_xMn_2O_4$ cells that contain a solid electrolyte of amorphous lithium phosphorus oxynitride (1-μm thickness). These cells can be cycled between 4.5 and 2.8 V at current densities of 10-20 mA/cm^2. Efforts are underway to reduce the impedance of the cell to operate at higher current densities.

PolyPlus Battery Co. was awarded a subcontract on the basis of a Request-for-Proposal (see below) to demonstrate the viability of Na/organosulfur (Na/SRPE) cells as practical components in batteries for EV applications. Components for Na/SRPE cells have been fabricated and evaluated in preliminary cycle tests.

Applied Science Research

Research projects at the Illinois Institute of Technology (IIT) and the Environmental Research Institute of Michigan (ERIM) are underway to develop corrosion-resistant materials for use in high-temperature batteries, such as Na/S and Li/FeS_2. IIT has undertaken a theoretical study of the evaporation process of $Mo(CO)_6$ to improve the quality of Mo_2C coatings obtained by plasma-enhanced chemical vapor deposition (CVD). The kinetic-gas theory was used to derive an equation that correlates the evaporation rate and the equilibrium pressure of $Mo(CO)_6$. ERIM has prepared TiN-coated Al containment materials by sputter-deposition techniques which were corrosion-resistant for 500 h in Na_2S_4 at temperatures up to 390°C. Another series of coatings, applied by ion-plating, showed no evidence of corrosion after 500 h in Na_2S_4 at 345°C.

Brookhaven National Laboratory (BNL) has used extended X-ray absorption fine structure (EXAFS) and X-ray absorption near-edge spectroscopy (XANES) to study nickel oxide electrodes that were cycled in Zn/NiOOH cells at LBL. EXAFS showed a substantial amount of Zn is present in the nickel oxide electrodes, and the Zn EXAFS was different for the electrodes obtained from the three vendors. Doping of manganese oxides with Group VIB metal oxides (CrO_3, MoO_3, WO_3) was found to improve the rate capabilities of the electrode in an electrolyte consisting of $LiClO_4$/PC-DME.

Lawrence Livermore National Laboratory (LLNL) is evaluating the performance characteristics of Li-ion cells manufactured by Sony Corporation. The capacity and specific energy of cells that were charged to 4.2 V charging were about 1 Ah and >94 Wh/kg, respectively. Cells were cycled under the USABC Dynamic Stress Tests (DST). The cell voltage at the DST high-power-step (150 W/kg) decreased approximately linearly with cycle number and run time from about 250 to 200 minutes after 310 cycles.

Case Western Reserve University (CWRU) has used *in situ* spectroscopic techniques and thermal analysis to study the Li/organic electrolyte interface. Temperature programmed desorption (TPD) studies with lithium exposed to propylene carbonate (PC) suggested that the thermal desorption peaks are characteristics of a reaction that produces lithium carbonate. Evidence was also found by TPD to indicate that Li hydride may also be formed with deuturated PC.

Several subcontracts were awarded from a Request-for-Proposal issued by LBL on "Applied Research on Novel Components for Advanced Secondary Batteries" (also see above for description of subcontract with PolyPlus Battery Co.). Northwestern University (NU) was awarded two subcontracts to synthesize polymer electrolytes based on aluminosilicate-polymer hybrid electrolytes with

improved low-temperature performance and to apply molecular dynamics and Monte Carlo simulations to understand the conduction process in polymer electrolytes. A new hybrid polymer electrolyte has been synthesized and will be tested shortly. Theoretical models are being developed to determine the influence of temperature, ion species, polymer chain basicity, and interionic correlations on conduction and Li transport number in polymer electrolytes. CWRU proposed to develop novel polymeric materials for polymer electrolytes in rechargeable Li batteries. An effort is underway to synthesize sulfonated and phosphonated polybenzimidazole (PBI) polymers, and poly(4,5-dimethyleneimidazole and hydroxy imidazole) polymers. The University of Dayton was awarded a subcontract to synthesize and characterize new polymer electrolytes that contain crown ethers which could have a fundamentally different mode of ion transport than those currently under investigation. The systems proposed are doped polymers with side chains that are terminated with crown ether groups which will complex with a lithium salt. It is hypothesized that these materials will create highly ordered structures, thereby forming paths through which ions can move easily. The synthesis of the three polymers involving a seven-step procedure has been initiated. Rutgers University is synthesizing polymer electrolytes by sol-gel processing of alkali silicate components. Various lithia-silicate compositions have been prepared which were found to have ionic conductivities over the range from room temperature to 400°C that show some promise for test in Li batteries. The State University of New York (Binghamton) is investigating the synthesis of molybdenum oxides for positive electrodes in rechargeable Li cells. Mo oxides ($M_xMoO_{3+x/2}$, where M = cation) were synthesized using the hydrothermal method at 150-200°C. Layered structures were obtained which should allow for rapid diffusion of Li ions. SRI International is developing high-performance hexathiobenzene-based organosulfur electrodes for Na cells. Electrodes and polymer electrolytes for Na/polyorganosulfide cells with PEO electrolyte have been fabricated.

Air Systems Research

Eltech Research Corporation is investigating the viability of bifunctional air electrodes that contain two electrocatalysts–one for oxygen evolution and the other for oxygen reduction. Electrodes with a graphitized acetylene black for the support and $NiCo_2O_4$ and either CoTMPP or $La_{0.6}Ca_{0.4}CoO_3$ as electrocatalysts have operated for over 100 cycles in 35 wt% KOH at room temperature.

Los Alamos National Laboratory (LANL) was awarded U.S. patents describing the developments in membrane catalyst layers for fuel cells (No. 5,211,984, issued May 18, 1993) (No. 5,234,777, issued Aug. 10, 1993) and the use of the thermoplastic (TBA^+) form of the ionomer (No. 5,234,777, issued Aug. 10, 1993). The first licensing agreement has been signed with a U.S. industrial company to utilize LANL technology for membrane/electrode assemblies in polymer electrolyte fuel cells. The use of Pt-Ru anodes and their tolerance to CO and CO_2 was investigated. The study showed that the advantage of Pt-Ru is not to enhance the oxidation of CO, but rather to minimize the extent of the CO_2 reduction process(es). Freeze-thaw cycle tests of PEM fuel cells showed no deleterious effect on performance. These results suggest that the direct application of a thin-film catalyst to the membrane generates a very good bond between catalyst and membrane to effectively prevent delamination under the demanding freeze-thaw cycling conditions. A new flow-field design for PEM fuel cells which contains a macroporous flow field for the reactant gases was tested. Higher limiting currents were obtained than in cells with ribbed flow fields. The removal of the gas diffusion anode backing layer dramatically improved the performance of a direct methanol fuel cell at 80°C, with both liquid and vapor feeds.

BNL is utilizing X-ray absorption spectroscopy (XAS) to study the adsorbed Pb on Pt catalysts. The results suggest that the electrocatalysis of small organic molecules on Pb-modified Pt cannot be attributed to adsorption of oxygen species on Pb, rather it must be because of the disordered nature of the Pb adlayer.

Future Directions

Transfer of the LBL Zn/NiOOH cell technology to Acme Electric Corporation has not been very successful. However, LBL has signed a CRADA with Energy Research Corporation to collaborate in an effort to transfer this technology. A new project was initiated with Southern University to utilize EXAFS to study iron sulfides for electrode materials.

References

Kinoshita K, *et al.* Exploratory technology research program for electrochemical energy storage -annual report for 1993. Lawrence Berkeley Laboratory Report No. LBL-35567, October 1994.

Kinoshita K, Landgrebe A. Analysis of power and energy for fuel cell systems, *J. Power Sources*, 47:159 (1994).

Kinoshita K, Cairns E. *Fuel cells, encyclopedia of chemical technology*, Volume 11, New York: John Wiley & Sons, 1994; 1098-1121.

Cairns EJ. Advanced batteries for electric vehicles. Paper No. 130, 186th Meeting of the Electrochemical Society, Miami, FL, October 1994.

McLarnon FR. Exploratory technology program for electrochemical energy storage. Presentation at Annual Automotive Technology Development Contractors' Coordination Meeting, Dearborn, MI, October 1994.

Advanced Electrode Research

E.J. Cairns, F.R. McLarnon, T.C. Adler, E. Bidóia†, Y. Choi, D. Marmorstein, M.L. Perry, J.A. Reimer, P.N. Ross*, B. Rush, K.A. Striebel, and M.S. Yahnke*

We have been studying the behavior of electrodes used in advanced secondary batteries and fuel cells currently under development for energy storage applications. In addition, we have been investigating practical means for improving the performance and lifetimes of these batteries and fuel cells. Systems of current interest include ambient-temperature, alkaline-electrolyte rechargeable cells with Ni electrodes (Hydride/NiOOH, Zn/NiOOH); ambient-temperature, nonaqueous-electrolyte rechargeable cells with Li electrodes (Li/polymer, Li-ion); and fuel cells that utilize the direct electrooxidation of methanol. We study life-limiting and performance-limiting phenomena under realistic cell operating conditions.

*Materials Sciences Division, LBL
†Visiting scientist

Investigations of Methods to Improve the Lifetime of the Zinc/Nickel Oxide Cell

The rechargeable alkaline Zn/NiOOH cell is an attractive alternative to Cd/NiOOH (nickel/cadmium) and MH/NiOOH (nickel/metal-hydride) cells because it offers higher specific energy at significantly lower cost and is environmentally benign. It has been projected that the Zn/NiOOH battery can meet all of the mid-term performance and cost goals set by the U.S. Advanced Battery Consortium (USABC) for electric vehicle (EV) batteries, however prior versions of Zn/NiOOH batteries have exhibited lifetimes of only 100-200 deep discharge cycles. The life-limiting factor has been the rapid redistribution of active material (known as shape change) on the Zn electrode caused by the high solubility of Zn species in the 7M KOH electrolyte that was used. We have demonstrated that this shape-change problem can be largely eliminated by using electrolytes that have low Zn species solubility. Electrolytes with 3-5M KOH concentrations supplemented by the addition of F^- and CO_3^{2-} anions can extend the cycle-life of Zn/NiOOH cells to 500-600 cycles before the cells lose 40% of their initial capacities. These results were obtained in cells using an electrolyte consisting of 3.2M KOH, 1.8M KF and 1.8M K_2CO_3. Our tests also demonstrated that these cells can recover from severe overcharge and over-discharge excursions. Furthermore, they have been successfully discharged using the so-called USABC Dynamic Stress Test and the USABC Peak Power Test.

We have now carried out additional cell cycle-life testing using electrolytes with a range of KOH and anion concentrations to determine the functional limits of this class of electrolytes. Three 1.35-Ah cells were prepared with fixed anion concentrations of 1.8M KF and 1.8M K_2CO_3, while the KOH concentration was varied. Cells were cycled at 100% DOD until 20% of the initial cell capacity was lost. The cell with 5.5M KOH reached 220 cycles, the cell with 4.5M KOH reached 420 cycles and the cell with 3.5M KOH reached 385 cycles. Thus the 4.5M KOH - 1.8M KF - 1.8M K_2CO_3 electrolyte is considered to be near-optimal and is recommended for evaluation in larger cells. To determine if very low concentrations of anions would be effective a cell was tested with 4.5M KOH - 0.1M KF - 0.1M K_2CO_3 electrolyte; it lost 20% of its capacity after only 15 cycles, which indicates that large F^- and CO_3^{2-} anion concentrations are needed. A cell with 2.5M KOH - 5M KF - 1.5M K_2CO_3 electrolyte lost 20% of its capacity after 60 cycles, and another cell containing 3.5M KOH - 3.2M KF electrolyte achieved 180 cycles. These results indicate that the inclusion of significant amounts of OH^- and CO_3^{2-} ions in the electrolyte is important.

Conductivities of these electrolytes and others were measured at 25°C using a specially designed cell. It was found that pure aqueous KOH electrolyte exhibits a conductivity maximum at ~5.7M, and the conductivity of 4.5 M KOH electrolyte is ~90 % of this maximum value. The addition of F^- and/or CO_3^{2-} anions to 3.2 and 4.5M KOH electrolytes substantially decreases the ionic conductivity, contrary to our expectations. Saturation of the electrolyte with ZnO further reduces conductivity by complexing free OH^- ions. The exact manner in which the presence of these anions benefit the cell is not clearly understood. They may partially passivate the zinc electrode surface, or otherwise alter the kinetics of zinc dissolution and deposition, thereby modifying the current density distribution and impeding shape change,

A CRADA has been initiated with the Energy Research Corporation (ERC) of Danbury, CT. Using the LBL class of electrolyte ERC will develop 15-Ah and 150-Ah sealed cells, while LBL will provide research support by testing smaller-scale cells using the ERC lightweight roll-bonded NiOOH electrodes.

Novel Lithium/Polymer-Electrolyte/Sulfur Cells

Variants of Li/S cells have been under investigation since the 1950's, including systems as different as high-temperature (380-500°C) LiAl/FeS_2 cells and ambient-temperature Li/Li_2S_n (lithium polysulfide) cells. Interest in the Li/S couple stems from its high theoretical specific energy (~2600 Wh/kg) as well as its environmentally benign components. In principle, this system is well-suited to EV applications, however a practical Li/S battery showing promise for EVs has not been developed. Problems have ranged from positive-electrode swelling to dissolution of partially-reduced active material (polysulfides) into the electrolyte. These problems have resulted in low utilization of active material, short cell lifetimes, and low delivered specific energy and specific power. The recent development of polymer electrolytes with acceptable ionic conductivity has created a new opportunity for the development of a solid-state Li/S cell with high specific energy and high specific power. Related research at LBL (S.J. Visco, M.M. Doeff, and L.C. DeJonghe, Materials Science Division) has led to the development of Li/polyorganodisulfide (-(SRS)$_n$-) cells, however the specific energy of the Li/SRS battery may not be sufficiently high to meet long-term USABC goals. The development of a functional positive electrode utilizing elemental sulfur should, however, provide the basis for a viable EV battery.

Our preliminary investigation of this class of cells began with the preparation of thin-film (~100s of μm) positive electrodes composed of sulfur, carbon black, polyethylene oxide complexed with a lithium salt, and a carbon dispersant. Cells have been assembled with these electrodes, and galvanostatic experiments resulted in well-behaved charge and discharge cycles. Utilization of the active material has, however, been poor. Investigation of means for improving the utilization of the sulfur is currently being pursued, involving morphological studies of the electrode and the development of chemical and physical methods for improving contact between phases. Future work will include studies of surface reactions taking place during charge and discharge.

Effect of Electrocatalyst and Electrolyte Composition on Methanol/Air Fuel Cell Performance

Fuel cells offer the promise of higher energy conversion efficiency and greatly reduced emissions, compared to combustion engines, and they are being developed for use in electric vehicles. However, present-day fuel cells operate on H_2, so either a H_2-storage device or a reformer must be carried on-board the vehicle. Each of these H_2-delivery options results in a heavy, bulky, costly, slow-reacting, and complex fuel-cell power plant. There is a strong need to develop a fuel cell that can electrochemically oxidize liquid fuels, and the successful development of a direct-methanol fuel cell (DMFC) would represent a major advance for fuel-cell-powered vehicles. However, some major obstacles must be addressed before acceptable performance can be attained with DMFCs. The oxidation rate

of CH_3OH is several orders of magnitude lower than that of H_2 on a Pt catalyst, and oxidation products other than the expected H_2O and CO_2 were observed in some cases. The problem of the slow oxidation rate of CH_3OH has been partially addressed by utilizing bimetallic catalysts. Previous work in this laboratory has confirmed that a Pt/Ru catalyst supported on graphitized carbon has a significantly higher catalytic activity for the oxidation of CH_3OH than supported Pt alone.

Cathode deactivation and the formation of CH_2O in acidic electrolytes, and the unwanted formation of carbonates in hydroxide electrolytes, have prompted previous researchers to study buffered electrolytes. Aqueous Cs_2CO_3 appears to be an electrolyte that does not suffer from the shortcomings of acidic and other alkaline electrolytes. The major goal of this research project is to demonstrate in a realistic system that the electrooxidation of CH_3OH is efficient and produces only H_2O and CO_2 as reaction products. A model fuel cell was designed and fabricated to accommodate 20-cm^2 electrodes. Electrodes of various catalyst loadings and polytetrafluoroethylene content have been prepared and tested in both half-cell and full-cell configurations, utilizing both H_2SO_4 and Cs_2CO_3 electrolytes and H_2 and CH_3OH feeds. The electrodes have a bi-layered structure, consisting of a semi-hydrophilic reaction layer which is pressed onto a hydrophobic gas diffusion layer. The active surface area is 18-20 cm^2 with a metal loading of 0.3 to 0.5 mg/cm^2. Recent efforts have addressed various problems including electrolyte seepage through the electrodes, inadequate catalyst wetting and possible catalyst poisoning. Future experiments will seek to optimize DMFC performance by varying the composition of the electrode and electrolyte, and adjusting the operating temperature (80-140°C). Analyses of the exit gases will be performed to determine if CH_3OH oxidizes completely to benign reaction products. An examination of an optimized system will be performed to ascertain its suitability for electric vehicles and other applications.

Poisoning of Fuel Cell Electrocatalyst Surfaces: NMR Spectroscopic Studies

Platinum is the most active single-component catalyst for CH_3OH electrooxidation in DMFCs; however, poisoning reactions on the catalyst surface in acidic electrolytes render the anode ineffective under target operating conditions. As an approach to designing better catalysts for this system, a number of *in situ*, *ex situ* and on-line techniques have recently been utilized to obtain information on the nature of the poisoning species. While significant advances have been made toward this end, no current technique can yield information on practical (supported, dispersed) electrocatalysts via *in situ* analysis.

Nuclear magnetic resonance (NMR) spectroscopy is a quantitative, non-destructive, bulk method of probing the chemical environment of a specific nucleus. In the last two decades the technique has been used successfully in the field of gas-phase catalysis as a tool for identifying and characterizing chemisorbed species on practical catalysts. Our research seeks to extend the application of NMR spectroscopy to studies of surface poisoning of carbon-supported Pt and Pt-alloy DMFC anodes.

For these experiments, we have designed and constructed a glass three-electrode electrochemical cell for use in a narrow-bore (5 cm) spectrometer operating at a proton frequency of 270 MHz (illustrated on p. 6 of the *Energy Conversion & Storage Program 1993 Annual Report*, LBL-35242). The working electrode material is commercially obtained and is composed of 20wt% Pt on Vulcan XC-72 carbon. These catalyst particles are further supported on a thin carbon cloth. This cloth is rolled tightly to form a cylindrical porous plug, filling the working electrode chamber inside of the NMR transmitter/receiver coil with an active catalyst surface area of ~3 m^2.

We have carried out preliminary studies on a model system of adsorbed CO. Lending justification to this choice are results of *in situ* infrared studies of smooth Pt electrodes which have suggested CO as the main poisoning adsorbate in the CH_3OH reaction. We have set up a flow system for adsorption of ^{13}C-enriched CO from CO-saturated aqueous H_2SO_4. Because CO is irreversibly adsorbed on the Pt surface, we are able to monitor adsorption indirectly by voltammetrically observing the suppression of H adsorption (Fig. 1). Our current efforts are focused on the detection and isolation of the ^{13}C NMR signal arising from ^{13}CO adsorbed on the electrodes described above under open-circuit conditions. With these initial studies we hope to establish the feasibility of NMR for providing *in situ* information on species adsorption at the electrode-electrolyte interface. We will then have a firm base for studying surface poisoning in the CH_3OH electrooxidation reaction.

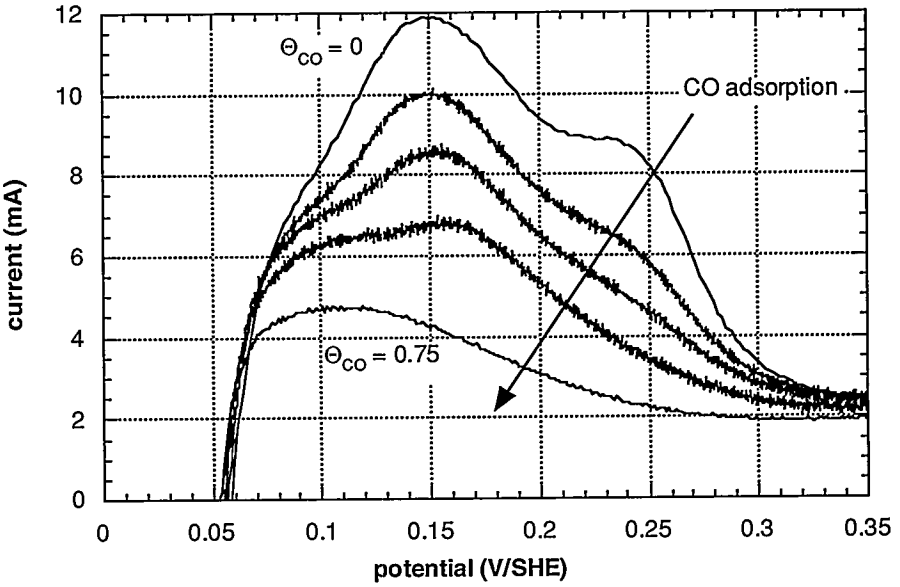

Fig. 1. *Electrochemical monitoring of CO adsorption onto carbon-supported Pt electrocatalysts. Sweep rate = 0.2 mV/s, electrolyte is 3M H_2SO_4.*

Application of Photothermal Deflection Spectroscopy to The Study of Electrochemical Interfaces

The purpose of this work is to use *in situ* Photothermal Deflection Spectroscopy (PDS) to study CH_3OH electrooxidation on a Pt electrode surface. With PDS, we can measure the absorption spectrum of the electrode surface and simultaneously detect concentration gradients in the electrolyte, thus allowing us to better understand the mechanism of the electrooxidation reaction. We have carried out initial experiments using probe beam deflection to detect the electrolyte concentration gradients that accompany the formation and removal of platinum oxide films. We have found that the deflectograms (graphical output from the probe beam deflection signal) for three acidic media (H_3PO_4, H_2SO_4 and $HClO_4$) show slight differences due to specific anion adsorption on the electrode surface. However, we discovered that the deflectogram changes its shape remarkably for an electrolyte contaminated by trace amounts of metal ions, as shown in Fig. 2. In comparing PDS results to those obtained with cyclic voltammetry, we found PDS to be more sensitive to metallic ion contamination on the Pt electrode; metal-ion concentrations of about 10^{-7} M can be detected by PDS.

Before PDS can be used to study the CH_3OH electrooxidation reaction on Pt electrodes, it is necessary to develop physically meaningful mechanistic models which are essential for the interpretation of electrode behavior. For this purpose, mathematical models which solve the diffusion equations for the time-varying flux boundary conditions at the electrode will be used to predict the concentration gradients and the corresponding electrolyte refractive-index gradients.

Direct Hydrocarbon Solid Polymer Fuel Cells

Solid-polymer-electrolyte fuel cells (SPEFCs) appear to be one of the most-promising systems for transportation applications due to their high power and energy density and low-temperature operation. Many researchers are investigating the possibility of a direct-methanol SPEFC because of problems such as on-board storage of H_2 or in-vehicle reforming of fuels such as CH_3OH. Although CH_3OH is one of the most electroactive organic fuels its performance in SPEFCs is significantly degraded by the undesirable crossover of fuel from the anode to the cathode. The crossover rate is substantial because of the affinity of the perfluorinated sulfonic acid (PFSA) membrane electrolyte for CH_3OH as well as water. Because CH_3OH and water are similar polar molecules, the prospect for developing a separator that can discriminate between them is not very promising.

The goal of this research project is to explore the possibility of a direct-hydrocarbon SPEFC. Because of the slow anodic oxidation rate of hydrocarbons, especially at low temperatures, such systems have not been examined in recent years. However, the same factors which have produced a significant improvement of fuel cell reaction kinetics with PFSA electrolytes, compared to other acids, may also significantly enhance the electrochemical oxidation rate of hydrocarbons. PFSA is a superacid and the anions are strongly hydrated in addition to being essentially immobilized by the membrane structure; this results in minimal anion adsorption on the electrocatalyst surface. Although the direct electrochemical oxidation rate of hydrocarbons will likely be substantially slower than that of H_2 or CH_3OH, the overall performance of a direct-hydrocarbon SPEFC may be justified by the convenience and low cost of using these

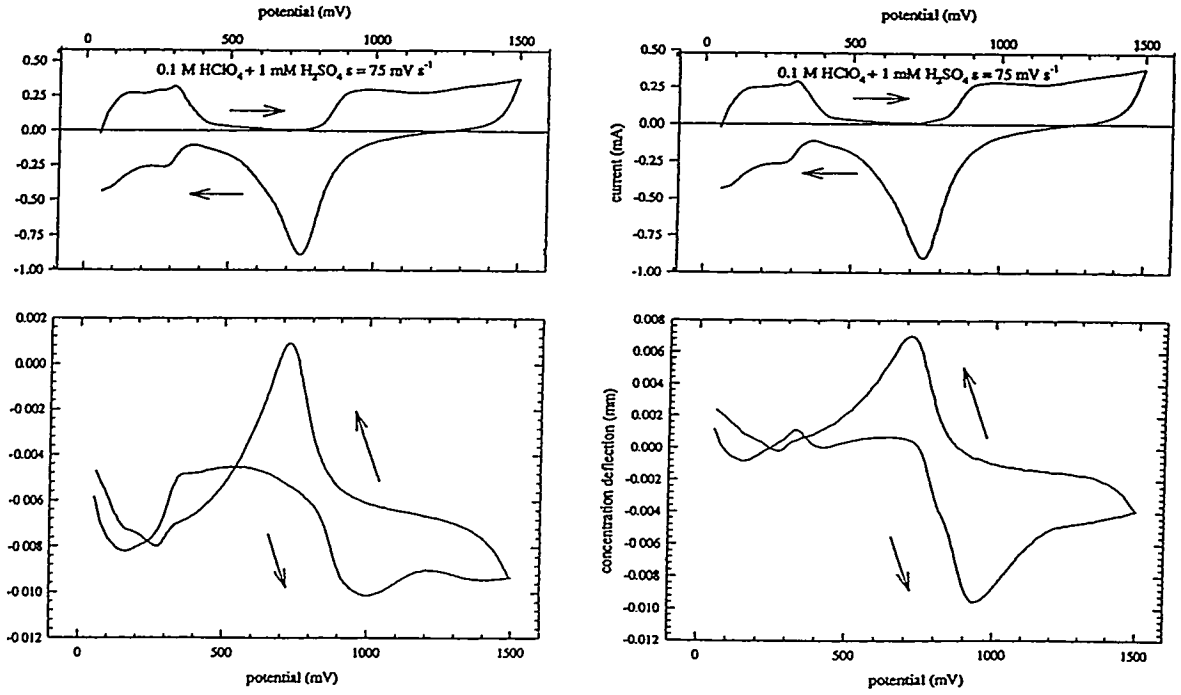

Fig. 2. *Voltammogram (upper panel) and corresponding deflectogram (lower panel) recorded on Pt at 24°C in 0.1 M $HClO_4$ + 1 mM H_2SO_4 electrolyte: (a) without contamination and (b) contaminated by metallic ions.*

fuels. Also, because hydrocarbons are non-polar, crossover should not be a significant problem in this system.

A model SPEFC was designed and fabricated to accommodate 20-cm^2 electrodes. Polarization tests utilizing H_2 fuel are underway to calibrate the cell performance. These results will be used as a comparison for future experiments with a variety of hydrocarbon fuels. The performance of alkanes and alkenes as well as mixtures of these fuels, such as natural gas, will be investigated. Analyses of the exit gases will be performed to determine if these fuels oxidize completely to benign reaction products. Experiments using electrocatalysts other than platinum will also be conducted with these fuels. An examination of the results will be performed to ascertain the feasibility of direct-hydrocarbon SPEFCs for electric vehicles and other applications.

References

Brisard GM, Rudnicki JD, McLarnon FR, Cairns EJ. Application of probe beam deflection to study the electrooxidation of copper in alkaline media. *Electrochim. Acta* 1995 (accepted for publication.

Gasteiger HA, Ross PN Jr, Cairns EJ. *Methanol electrooxidation on well-characterized Pt-Ru alloys.* Lawrence Berkeley Laboratory Report No. LBL-34894, November 1993.

Gasteiger HA, Ross PN Jr, Cairns EJ. LEIS and AES on sputtered and annealed polycrystalline Pt-Ru bulk alloys. *Surface Science.* 1993; 293:67.

Gasteiger HA, Markovic N, Ross PN Jr, Cairns EJ. Methanol electrooxidation on well-characterized Pt-Ru alloys. *J. Phys. Chem.* 1993; 97:12020.

Gasteiger HA, Markovic N, Ross PN Jr, Cairns EJ. CO electrooxidation on well-characterized Pt-Ru alloys. *J. Phys. Chem.* 1994; 98:617.

Gasteiger HA, Markovic N, Ross PN Jr, Cairns EJ. Electrooxidation of small organic molecules on well-characterized Pt-Ru alloys. *Electrochim. Acta* 1994; 39:1825.

Gasteiger HA, Markovic N, Ross PN Jr, Cairns EJ. Temperature-dependent methanol electro-oxidation on well-characterized Pt-Ru alloys. *J. Electrochem. Soc.* 1994; 141:1795.

Kinoshita K, Cairns EJ. Fuel Cells. *Encyclopedia of Chemical Technology* 1994; 11:1098.

Plivelich RF, McLarnon FR, Cairns EJ. *Nickel hydroxide electrodes in reduced-alkalinity electrolytes.* Lawrence Berkeley Laboratory Report No. LBL-35628, April 1994.

Plivelich RF, McLarnon FR, Cairns EJ. Degradation mechanisms of nickel oxide electrodes in zinc/nickel oxide cells with low-zinc-solubility electrolytes. *J. Appl. Electrochem.* 1995 (accepted for publication.

Rauhe BR Jr, McLarnon FR, Cairns EJ. Direct anodic oxidation of methanol on supported platinum/ruthenium catalyst in aqueous cesium carbonate. *J. Electrochem. Soc.* 1995 (accepted for publication).

Taucher W, Adler TC, McLarnon FR, Cairns EJ. Lightweight nickel electrodes for zinc/nickel oxide cells. Paper presented at the 45th Meeting of the International Society of Electrochemistry, Porto, Portugal, August 1994.

Taucher W, Adler TC, McLarnon FR, Cairns EJ. Development of lightweight nickel electrodes for zinc/nickel oxide batteries. Paper no. 132 presented at the 186th Meeting of the Electrochemical Society, Miami Beach, FL, October 1994.

Electrode Surface Layers

F.R. McLarnon, R.H. Muller, and F.-P. Kong*

We are studying the effects of surface modification on the electrochemical behavior of electrodes used in rechargeable batteries. We use both low-energy (~3 keV) and high-energy (to >100 keV) ion beams to implant dopants into the surfaces of electrodes. Advanced spectroscopic ellipsometry and traditional electrochemical characterization methods are used to study the structure, composition and evolution of surface layers on these electrodes. The primary objective of this research is to identify film properties that improve the rechargeability, cycle-life performance, specific power, specific energy, and stability of electrochemical cells.

Our prior work demonstrated that Co additions to Ni electrodes significantly improves the extent of electrochemical interconversion between $Ni(OH)_2$ (predominant active species on a discharged Ni electrode) and NiOOH (predominant active species on a charged Ni oxide electrode), consistent with empirical evidence in porous battery electrodes. This beneficial outcome has been attributed to the electronic effects of Co dopants, *i.e.*, Co balances the conductivity difference between $Ni(OH)_2$ and NiOOH and thereby promotes a more uniform electrochemical reaction distribution and a more complete interconversion process.

Because the O_2-evolution reaction at the Ni electrode surface strongly competes with interconversion between Ni^{2+} and Ni^{3+} or other higher-valent Ni oxidation states, suppression of this unwanted parasitic reaction will lead to the improved coulombic efficiency, energy efficiency and specific energy of electrochemical cells utilizing of Ni electrodes. We have selected Au, Pb, Ta, Ti, W and Ti_4O_7 as dopants because of their relatively poor surface catalytic behavior with respect to O_2 evolution, however the effects of these species on electrochemical interconversions in Ni electrodes has not been well studied. A low-energy ion implantation technique known as Metal Plasma Immersion Ion Implantation (MPIII) has been chosen to enhance the surface effect related to the O_2-evolution reaction. The MPIII electrode bias potential and the duty cycle of the substrate bias pulser were controlled at -2kV (the beam energy varies from 3.2 to 6.2 keV depending on the mean ion charge for individual elements) and 25%, respectively, to produce an ion-penetration depth of ~2-3 nm. The dose levels of implanted ions were estimated to be 4×10^{15} - 2×10^{16}, which implies that the atomic fraction of foreign atoms at the electrode surface is ~30%.

Preliminary tests showed that the overpotential for O_2 evolution at the surface of a Ti_4O_7-implanted Ni electrode is increased by 50-105 mV, compared with electrodes implanted with other elements. However this suppression of O_2 evolution did not result in a better electrode performance. Of the doping materials investigated thus far, Au, W, and Pb performed the best with respect to

*Materials Sciences Division, LBL

overall charge/discharge characteristics. Deconvolution of the measured *in-situ* ellipsometric spectra allowed us to quantitatively analyze the interconversion between $Ni(OH)_2$ and NiOOH. We estimate the initial charge efficiency of an Au-implanted electrode to be ~90%, but it drops to ~30% during the charging process. These values are significantly lower than those obtained in the electrode with Co additives by high-energy ion implantation techniques. This fact suggests that the bulk effects rather than surface effects may play a more important role in porous Ni battery electrodes.

Experiments to further characterize ion-implanted Ni electrodes will continue. The increase in the O_2 evolution overpotential caused by the implantation of Ti_4O_7 is encouraging, but the mechanism of Ni oxidation in such electrodes must be studied to understand the lack of increased performance in the Ti_4O_7-implanted electrode.

References

Zhang ST, Kong FP, Muller RH. Effect of Ion Implantation on the corrosion behavior of lead and a lead-antimony alloy. *J. Electrochem. Soc.* 1994; 141:2677.

Anders S, Anders A, Brown I, Kong F, McLarnon F. Surface modification of nickel battery electrodes by cobalt plasma immersion ion implantation and deposition," Paper presented at the Second International Workshop on Plasma Based Ion Implantation, Sydney, Australia, February 1995.

Analysis and Simulation of Electrochemical Systems

J. Newman

This program involves fundamental investigations of the transport and interfacial phenomena important in electrochemical systems. Results of this work are used to analyze experimental data, to identify important system parameters, and to aid in the design and scale-up of electrochemical systems. The approach taken is to develop a detailed mathematical model of the device using the principles of transport phenomena, reaction kinetics, and thermodynamics. The mathematical models are developed to be as general as possible without unnecessary mathematical or physical approximations. The resulting sets of coupled equations are then solved numerically which permits the complex interactions between phenomena to be treated. Experimental work may then be used to confirm and refine the mathematical models and to determine the physical parameters necessary for a complete, quantitative understanding of the system.

Lithium-based rechargeable batteries have been explored in detail using mathematical modeling. The first generation model has now been expanded to treat film formation on the electrode surfaces and temperature rise during nonisothermal discharges. The model is also able to simulate more complicated charge/discharge schemes than just galvanostatic, such as potentiostatic taper charges, power pulses, and extended cycling. The specific Li systems that are being explored include a Li foil cell consisting of a polymer electrolyte and a manganese oxide spinel positive electrode. This system has been studied in detail in order to determine the tradeoffs in system performance that occur as the transport properties of the polymer electrolyte, especially ionic conductivity and Li ion transference number, are varied.

Several Li-ion battery systems have also been explored in detail with the mathematical models due to these systems' popularity in the literature and recent commercial successes. A dual Li-ion battery consisting of a carbon negative electrode, nonaqueous liquid solvent, and manganese oxide spinel positive electrode has been studied. The optimization of this system for consumer electronic and electric-vehicle applications is discussed. The behavior of the Sony phone cell has also been explored, with particular attention to the capacity-rate behavior and the relaxation processes during rest periods. Due to the relatively large diffusion coefficient of Li salts in the liquid solvents, these systems do not exhibit the extreme solution-phase diffusion limitations seen in polymer electrolyte systems. Instead, these liquid solvent systems tend to be ohmically-dominated, which may make their behavior easier to understand and their optimization straightforward.

The modeling work also emphasized the importance of accurate transport property data for the design process. The necessary transport properties are rarely available for even the most common Li salt and solvent combinations. This problem is even worse for solid polymer electrolytes where the methodology to measure the Li ion transference number without the assumption of a dilute, ideal solution does not exist. This situation motivated an experimental project to measure a complete set of transport properties for a given polymer electrolyte over a wide range of salt concentrations. A novel method to measure the Li ion transference number was developed that is easy to carry out and involves no poor assumptions about the ideality of the solution. These experiments were performed on sodium trifluoromethane sulfonate in polyethylene oxide at 85°C. The transport properties were found to depend strongly on the salt concentration. The sodium ion transference number decreased sharply from around 0.3 in the most dilute solution to large negative values ($t_+^0 = -4$) at higher salt concentrations, which indicates the existence of ion-association processes in this solution. The mean molar activity coefficient of the salt confirms that this solution is highly nonideal. The methodology that was developed is currently being applied to various Li salts in polyethylene oxide.

Thermal modeling of Li/polymer cell stacks has been carried out for electric-vehicle applications. This work has focused on the coupling of heat generation and transport to the electrochemical processes occurring inside of individual cells. The complexity of this mathematical problem prevents an exact numerical solution from being developed, so various approximate techniques for treating this coupling have been explored. For polymer electrolyte systems, where operation at elevated temperatures is necessary to have sufficient ionic conductivity, strict temperature control of the cell stack is critical.

Other ongoing modeling projects include simulations of electrochemical capacitor devices and metal hydride batteries. The charge and discharge of electrochemical capacitors, including so-called "supercapacitors" and the effects of pseudocapacitance, is being explored under various operating conditions. The utility of these devices for high-power

applications will be evaluated and compared to other alternatives such as ultrathin lead-acid batteries. A comprehensive, full-cell sandwich model of the metal hydride battery is under development and will be used to study the performance and optimization of this system for electric-vehicle applications.

References

Fuller TF, Newman J. "Electrochemical processing (Introduction)," Mary Howe-Grant, ed. *Kirk Othmer Encyclopedia of Chemical Technology*, 4th ed., vol. 8, pp. 111-123 (John Wiley & Sons, Inc., 1994). LBL-33602, February 1993.

Fuller TF, Doyle M and Newman J. Simulation and optimization of the dual lithium ion insertion cell. *J. Electrochem. Soc.* 141 (1994), 1-10. LBL-33426, May 1993.

Mao Z, White RE, Newman J. Theoretical analysis of the discharge performance of a NiOOH/H_2 Cell. *J. Electrochem. Soc.*, 141 (1994), 54-64.

Battaglia V, Newman J. Magnetic field effects in high-power batteries. I. The penetration of an electric field into a cylindrical conductor, *J. Electrochem. Soc.*, 141 (1994), 703-708. LBL-34096, May 1993.

Battaglia V, Newman J. Magnetic field effects in high-power batteries. II. Time constant of a radial circuit terminated by a cylindrical cell with inductance *J. Electrochem. Soc.*, 141 (1994), 708-713. LBL-34097, May 1993.

Fuller TF, Doyle M, Newman J. Relaxation phenomena in lithium-ion-insertion cells. *J. Electrochem. Soc.*, 141 (1994), 982-990. LBL-34471, October 1993.

Doyle M, Fuller TF, Newman J. The importance of the lithium ion transference number in lithium/polymer cells. *Electrochim. Acta*, 39 (1994) 2073-2081. LBL-34378.

Fuller TF and Newman J. "Diffusion," *Encyclopedia of Chemistry* (Macmillan Publishing Co.), submitted. October, 1992.

Battaglia V, Newman J. Modeling of a growing oxide film: The iron/ironoxide system. July 20, 1993, LBL-34385. *J. Electrochem. Soc.*, submitted.

Fuller TF, Newman J. Metal hydride electrodes. August, 1993, LBL-34390. *Modern Aspects of Electrochemistry*, submitted.

Rush BM, Newman J. Periodic behavior in the iron/sulfuric acid system. I: Observations and a periodic mechanism. LBL-35637, June 1994. *J. Electrochem. Soc* submitted.

Rush BM and Newman J. Periodic behavior in the iron/sulfuric acid system. II: Coherence. LBL-35638, June 1994. *J. Electrochem. Soc.*, submitted.

Doyle M, Newman J. Modeling the performance of rechargeable lithium-based cells: design correlations for limiting cases. LBL-35712. *J. Power Sources*, Proceedings of the 7th International Meeting on Lithium Batteries, May 1994, submitted.

Doyle M, Reimers J, Newman J. A quick method of measuring the capacity *versus* discharge rate for a dual lithium ion insertion cell undergoing cycling. LBL-35024, April 1994. *J. Power Sources*, accepted.

Newman J. Optimization of porosity and electrode thickness with a reaction-zone model. LBL-35584, May 1994. Prepared for the Douglas N. Bennion Memorial Symposium, San Francisco Meeting of the Electrochemical Society, May 25, 1994.

Pals C, Doyle M, Fuller TF, Newman J. "Modeling of adiabatic and isothermal galvanostatic discharge behavior of the lithium/polymer/insertion cell," Prepared for the Douglas N. Bennion Memorial Symposium, San Francisco Meeting of the Electrochemical Society, May 25, 1994. LBL-35583.

Newman J. Optimization of porosity and electrode thickness with a reaction-zone model. LBL-35714, June 1994. *J. Electrochem. Soc.*, accepted.

Wang M-H and Newman J. The electrical conductivity of sodium polysulfide melts. LBL-35751, June 1994. *J. Electrochem. Soc.*, accepted.

Ma YP, Doyle M, Fuller TF, Doeff MM, De Jonghe LC and Newman J. The measurement of a complete set of transport properties for a concentrated solid polymer electrolyte solution. LBL-35026. August 1994. *J. Electrochem. Soc.*, submitted.

Newman J. Thermoelectric effects in electrochemical systems. LBL-36118, September 1994. *Ind. Engr. Chem. Research*, submitted.

Pals C, Newman J. Thermal modeling of the lithium/polymer battery I. Discharge behavior of a single cell. LBL-36294, November 1994 submitted.

Pals C, Newman J. Thermal modeling of the lithium/polymer battery II. Temperature profiles in a cell stack. LBL-36295, November 1994. *J. Electrochem. Soc.*, submitted.

Carbon Electrochemistry

K. Kinoshita and X. Song

A project was initiated to identify the critical parameters that control the reversible intercalation of lithium in carbonaceous materials and to determine their maximum capacity for lithium intercalation. One of the attractive features of using lithium-intercalated carbon rather than lithium metal itself as the negative electrode in batteries is related to safety. Carbonaceous materials which can efficiently intercalate (charge) and de-intercalate (discharge) lithium are not prone to some of the safety hazards (*i.e.*, explosions, venting) that have been encountered with metallic lithium electrodes in rechargeable batteries. In addition, electrodes consisting of lithium intercalated carbon can be repeatedly charged/discharged over many cycles in nonaqueous electrolytes.

Studies on the intercalation of lithium in carbonaceous materials were conducted in collaboration with LLNL. Samples obtained from commercial vendors, as well as several that were synthesized in-house, were investigated. A systematic study of the physical properties was undertaken utilizing electron microscopy (facilities at the National Center for Electron Microscopy) and x-ray diffraction analysis at LBL. These carbons were fabricated into electrode structures and the electrochemical intercalation of Li in nonaqueous electrolytes was studied at LLNL. Synthetic graphites, with d(002) spacing of 0.3354 nm, obtained from Lonza yielded the theoretical capacity for Li intercalation (LiC_6), whereas non-graphitized carbonaceous materials were able to intercalate only about 50% of the theoretical amount. However, petroleum coke that was doped with phosphorus showed enhanced Li intercalation. Carbon black which was heat treated to form a

graphitic structure, with a d(002) spacing of 0.344 nm, did not intercalate as much Li as the initial sample. This result appears to contradict the findings with the synthetic graphites. A closer analysis of the intercalation mechanism is underway and suggests that the mechanism may differ between the highly ordered graphites and the less ordered carbons. Initial analysis of published data indicates that the intercalation of Li is lower with carbons that have a d(002) spacing of about 0.345 nm, than materials with higher or lower d-spacing. This finding suggests that the mechanism for Li intercalation may differ with graphitic materials, d(002) < 0.345 nm, and with the disordered carbons, d(002) > 0.345 nm.

EXAFS Studies of Electrode Materials for Lithium Batteries

E.J. Cairns, S.P. Cramer, and C. Horne

The purpose of this research is to obtain a thorough understanding of the lithium intercalation process at the atomic level by employing *in-situ* x-ray spectroscopic techniques such as Extended X-ray Absorption Fine Structure (EXAFS) combined with electrochemical characterization. There has been an increasing emphasis on high-specific-energy lithium batteries for a variety of power source requirements. Manganese oxides intercalate lithium and also possess low equivalent weight, cost, and toxicity, making them ideal candidates for lithium battery positive electrodes. However, irreversible structural and chemical changes in the manganese oxide host lattice upon lithium intercalation reduce battery cycle life necessitating improvements in material design and a deeper knowledge of the intercalation mechanism in these materials. With this insight, synthesis and operation of active materials under conditions that provide maximum utilization and cycle life are possible, resulting in batteries of higher specific energy, longer life, and greater commercial interest.

Work this first year centered on proving the applicability of EXAFS to characterize structural changes associated with lithium intercalation. The cell chosen for this preliminary work consisted of lithium foil negative electrode, $(PEO)_8LiCF_3SO_3$ electrolyte, and $Li_2Mn_4O_9$-based positive electrode. $Li_2Mn_4O_9$ is a spinel oxide that has been the subject of research at LBL as well as a number of other laboratories around the world for use in lithium batteries. The open-circuit potential of $Li_2Mn_4O_9$ *vs* Li metal is 3.25V and the theoretical capacity is 213 mAh/g, corresponding to the discharge reaction:

$$Li_2Mn_4O_9 + 3\,Li^+ \longrightarrow Li_5Mn_4O_9.$$

A positive-electrode design was needed to balance the electrochemical and spectroscopic requirements of the experiment. Electrochemically, a high spinel content is desired to maximize specific energy whereas spectroscopically, large Mn concentrations can cause self-absorption, diminishing EXAFS signal intensity. Emission scans of positive electrodes containing different $Li_2Mn_4O_9$ concentrations, taken at Stanford Synchrotron Radiation Laboratory (SSRL), revealed sufficient signal intensity over a concentration range of 10 to 50 w/w.

After establishing an appropriate electrode design, EXAFS measurements were performed at SSRL Beamline 4-1 to probe the spinel structure as a function of intercalated state. The manganese oxidation state in $Li_2Mn_4O_9$ is +4. As Li^+ ions intercalate into the spinel, the Mn oxidation state is reduced, reaching +3.25 when $Li_2Mn_4O_9$ is fully discharged to $Li_5Mn_4O_9$. A Jahn-Teller distortion occurs when the Mn oxidation-state falls below +3.5, corresponding to $Li_{4.4}Mn_4O_9$, changing the spinel's cubic symmetry to tetragonal to accommodate Li^+ into the structure. Three positive electrodes, one undischarged, one discharged to $Li_{3.7}Mn_4O_9$ (Mn +3.6), and another discharged to $Li_{4.4}Mn_4O_9$ (Mn +3.4), were evaluated. Electrode discharging was performed at LBL; the Li foil/PEO separator/positive electrode assembly was removed from the cell following discharge.

Preliminary EXAFS analysis of Mn K edge fluorescence spectra from the three electrodes gives the Fourier Transforms shown (Figure). The broadening of the two main peaks is indicative of structural changes caused by Li^+ incorporated during discharge. The position of the first peak agrees with that expected for oxygen octahedra surrounding the Mn based on X-ray diffraction data, whereas the second peak is attributed to Mn and Li. In addition, scans taken at different locations on the electrode discharged to $Li_{3.7}Mn_4O_9$ showed nearly identical Fourier Transforms. Analysis is ongoing to identify the type and number of atoms giving rise to the coordination shells seen (Figure).

Recently, a high-resolution oxidation-state specific EXAFS technique was demonstrated for the first time by the Cramer Group on Mn-containing

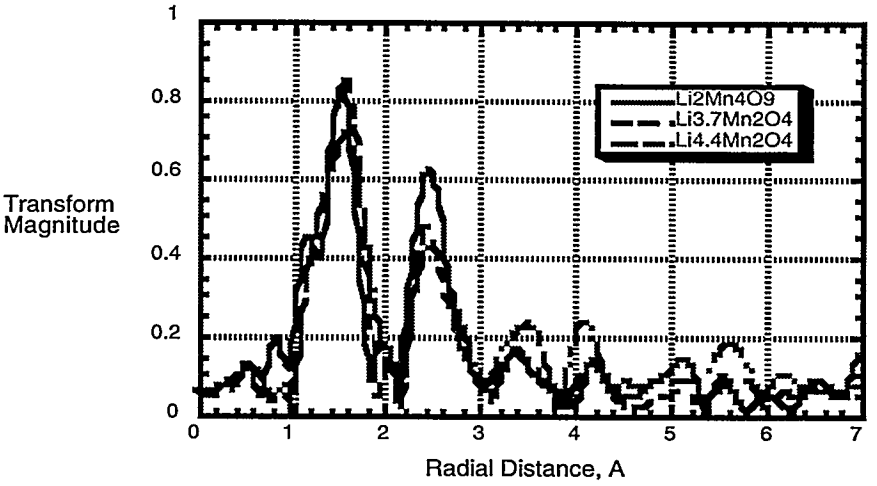

Figure. *Fourier Transform of Mn K-edge fluorescence of electrode states: $Li_2Mn_4O_9$, $Li_{3.7}Mn_4O_9$, and $Li_{4.4}Mn_4O_9$.*

metalloproteins. This technique differs from conventional EXAFS in that only K_b radiation is measured rather than that from all K transitions, K_a being the major component. Because K_b radiation originates from 3p—> 1s transitions, its EXAFS modulations are more sensitive to changes within the 3d orbitals, the valence orbitals of Mn, than K_a radiation emitted from 2p —> 1s transitions. This makes the chemical shift of K_b emission more resolvable and allows collection of radiative intensity modulations when focusing the detector on K_b wavelengths corresponding to a specific oxidation state. This technique allows the determination of local structure for each Mn oxidation state within the sample. High-resolution spectrometers are required to enhance K_b signal strength given the order-of-magnitude lower intensity as compared to K_a. The data shown in the Figure were collected on conventional EXAFS equipment; the structures correspond to that averaged around all Mn within the electrode. This past year, emission intensity of the electrode discharged to $Li_{4.4}Mn_4O_9$ was measured on the high-resolution spectrometer and signal strength was sufficient for EXAFS analysis. These experimental results prove the ability of EXAFS to characterize the structural differences within intercalation electrodes and the viability of the high-resolution technique.

The upcoming year will focus on applying high-resolution, oxidation-state specific EXAFS to Li-Mn-O spinel electrodes. Conventional EXAFS is scheduled to continue at SSRL in February 1995 and will provide a foundation for high-resolution measurements scheduled to commence in March 1995 at National Synchrotron Light Source Beamline X-25. *In-situ* measurements are planned for the subsequent beam time allocation, expected in the second half of 1995.

Application of Pulsed Laser Deposition to the Study of Rechargeable Battery Materials

K.A. Striebel, C. Deng, and E.J. Cairns

The aim of this project is to study the performance-limiting phenomena of complex metal oxides, present in a wide variety of rechargeable batteries, and to suggest practical means for improving their performance and lifetime in secondary consumer batteries. We prepare thin dense films from these oxides on electronically conductive substrates with the pulsed laser deposition technique. This method is superior to other film-formation techniques, such as sputtering and vapor evaporation, based on both speed and simplicity. Smooth 300-nm films with complex stoichiometries can be prepared in 15 minutes from a single target. We have prepared films from metal oxide targets with the perovskite and rock-salt structures on substrates of glassy carbon, stainless steel, tantalum, nickel and titanium. Films are characterized with x-ray diffraction, x-ray absorbance, XPS, optical and scanning electron microscopy and profilometry. Electrochemical properties of the metal oxide films, such as the electrocatalyst kinetics, film corrosion behavior and active species diffusivity, can be measured with standard techniques for geometries with well-defined electrode-electrolyte interfaces.

Transition metal perovskites represent a class of complex metal oxides that may be useful as electrocatalysts in the bifunctional air electrode. The perovskites $La_{0.6}Ca_{0.4}MnO_3$ and $La_{0.6}Ca_{0.4}CoO_3$, have been prepared with pulsed laser deposition. Preliminary rotating ring-disk measurements studies indicate that they are not highly active electrocatalysts for O_2 reduction but they show very little production of the harmful intermediate peroxide. Another class of metal oxides, which are of great interest to lithium battery development, namely lithium intercalation oxides are also being studied. Films of Li_xCoO_2 were prepared on heated stainless steel substrates. They appear to be quite stable in propylene carbonate-based electrolyte. Electrochemical characterization of the diffusion and intercalation kinetics of Li^+ in Li_xCoO_2 is underway. Parametric studies of the pulsed laser deposition conditions required to make films of the pyrochlore electrocatalysts $Pb_2Ru_2O_7$ and $Bi_2Ru_2O_7$ are planned. These electrocatalysts are more active for O_2 reduction than the perovskites discussed above, but they also tend to be more unstable. In future work, electrocatalytic and intercalation metal-oxide films with preferred orientations will be prepared to further elucidate the effect of metal-oxide crystal structure on the electrochemical properties of interest. Efforts to prepare new metal oxides and to improve film density are underway.

Fundamental Characterization of Carbon-Based Materials for Electrochemical Systems

*K. Kinoshita, X. Chu, and N. Markovic**

A fundamental research program on the synthesis, characterization and modification of carbon-based materials to improve their properties for use in electrochemical systems was initiated. Oxygen reduction on various carbonaceous electrodes in aqueous electrolyte was studied using a ring-disk electrode system. Cyclic voltammograms from both the ring and the disk electrodes are monitored and related to the reaction mechanism. The effects of graphite surface pretreatment and modification on the O_2 reduction have been studied.

The experiments were carried out in a glass cell which has separate compartments for the reference and counter electrodes. A carbon electrode with an area of 0.28 mm^2 was mounted in a teflon holder of a ring-disk electrode. The ring electrode was gold, with a collection efficiency N of 0.25 as determined from the disk-ring geometry (radii). The ring electrode was typically set at +0.15 V *vs.* Hg/HgO, and 0.1 M KOH was used as the electrolyte.

In general it was observed that the high-density graphite sample (small grains randomly oriented) has a reasonably high activity over a wide range of

*Materials Sciences Division, LBL

applied potentials. However, anodic oxidation decreases the overall activity, and reduction of the oxidized electrode can not restore the activity. The freshly cleaved basal plane of high-oriented pyrolytic graphite (HOPG) has a little activity for O_2 reduction, about 10% of that for the high density graphite electrode. After oxidation of the basal plane of HOPG in air at 700°C for 1.0 hour, the surface showed no obvious change by scanning electron microscopy (SEM). However, the activity for O_2 reduction increases dramatically. This can be explained by the fact that heat treatment in air creates many surface defects such as monolayer pits. The O_2-reduction activity was also increased when 1,4 naphthoquinone was preadsorbed on the basal plane of graphite.

Future research effort will be concentrated on preparing carbon electrodes by carbonization of thermosetting polymer at a relatively low temperature. The type of doping agents and their concentration can be controlled. Therefore, the effect of heteroatoms and surface functional groups on the electrochemical properties of the modified carbon electrode will be evaluated.

Applied Research on Lithium/Polymer-Electrolyte Cells

E.J. Cairns, Y. Chen, T. Devine, Z. Deng, M. Doeff, J. Evans, D. Ghantous, L. Johnson*, J. Kerr, F. Kong, K. Kinoshita, F.R. McLarnon, J.S. Newman, L. Rao, T. Richardson*, P.N. Ross*, K.A. Striebel, M. Tian and S.-J. Wen*

LBL and the U.S. Advanced Battery Consortium have renewed their Cooperative Research and Development Agreement (CRADA) to investigate advanced Li/polymer-electrolyte battery technology for the third year. Research on the CRADA involves investigators from both the Energy and Environment Division and the Materials Sciences Division. Effort in the second year involved study of electrochemical phenomena at electrode/polymer-electrolyte interfaces, development of advanced mathematical models of Li/polymer-electrolyte cells, synthesis of improved polymer electrolytes and materials for positive electrodes, establishment of an extensive bibliographic database on components for Li/polymer-electrolyte cells, and investigation of overcharge/overdischarge phenomena in secondary Li cells. A new task was initiatied in the third year to study the corrosion of cell components in Li/polymer cells.

*Materials Sciences Division, LBL

Chemical Applications

Kinetic and Structural Studies of the Sulfidation of Large Particles of Lime and Limestone in Coal Gas

L.A. Fenouil and S. Lynn

Motivation

The development of reliable methods for removing solid and gaseous contaminants from coal-gas at high temperatures and pressures is one of the most important technological advances required in the field of coal gasification. Gaseous contaminants include H_2S, NH_3, and volatilized metal and alkali salts, all formed from trace components of the coal. Entrained solids are mainly gasifier fines formed during the gasification process. It is necessary that all of these be removed prior to the combustion of the coal gas to prevent damage to turbine equipment and infringement of emissions legislation.

This project explores the technical and economic feasibility of a high-temperature process for cleaning coal gas prior to combustion in a gas turbine. In the proposed process the coal gas would pass through a nearly-isothermal, moving bed of millimeter-size calcium carbonate (limestone) particles that would serve to remove particulates (by filtration), hydrogen sulfide (by chemisorption), and ammonia (by catalysis). Other configurations, such as entrained-flow, fluidized and packed-bed sorption systems are also under investigation. The objective of this research is to define the temperature at which these goals (mainly the sulfur removal) can best be realized at a given pressure and for a given coal gas composition, as well as to determine the performance of such a clean-up system.

Study of calcium-based sorbents under simulated coal gases

Thermodynamics

At a given fugacity of CO_2, limestone also undergoes calcination if the temperature is high enough (approximately 900°C for 1 bar of CO_2):

$$CaCO_3 \leftrightarrow CaO + CO_2 \qquad (1)$$

Below the calcination temperature of limestone the desulfurization reaction of importance is:

$$CaCO_3 + H_2S \leftrightarrow CaS + H_2O + CO_2 \quad (2)$$

which becomes increasingly favorable as the temperatures increases. Above the calcination temperature of $CaCO_3$, the lime (CaO) formed can then react with H_2S:

$$CaO + H_2S \leftrightarrow CaS + H_2O \qquad (3)$$

Reaction 2 is endothermic (about 165 kJ/mol at 900°C) whereas reaction 3 is exothermic (about 65 kJ/mol at 900°C). So, the lowest level of H_2S thermodynamically possible in a coal gas in contact with lime(stone) is obtained at the calcination temperature of the limestone, which is only a function of the partial pressure (*i.e.*, fugacity) of CO_2. However, it is favorable to operate the H_2S sorption reaction slightly above this temperature because of kinetic considerations, as we will see in the Results section. Extensive thermodynamic calculations show that the level of removal of H_2S could be well above the 90% mandated by the Clean Air Act, and often as high as 98%, for most modern coal-gasification systems (Fenouil, 1995).

Kinetics

All experiments were carried out with a differential tube reactor originally designed by Towler and described in earlier reports (Fenouil *et al.*, 1994). The conversion of $CaCO_3$ to CaO and CaS and of $MgCO_3$ to MgO was followed by a combination of gravimetric measurements and of iodometric titrations of CaS.

Results

Sorbent choice

The H_2S-sorption capabilities of 18-35 mesh particles (average mass-radius of 0.40 mm) of three different calcium-based sorbents (limestone, $CaCO_3$; dolomitic limestone, $[MgCO_3\text{-}CaCO_3]_1[CaCO_3]_3$; dolomite $MgCO_3\text{-}CaCO_3$) were tested under simulated coal gases. Two fundamentally different behaviors were observed.

Above the calcination temperature of $CaCO_3$, complete conversion of $CaCO_3$ to CaS can be achieved with all three sorbents (Fenouil and Lynn, 1995a). However, chemical attrition of the sorbent also increases as more magnesium is present. This chemical attrition, caused by near-explosive calcination of $MgCO_3$, is responsible for the formation of a relatively large quantity of fine powder. It thus appears that low-magnesium limestone, which has the best sulfur loading, should be the sorbent of choice. Nonetheless, dolomitic limestone and dolomite can also be used.

Below the calcination temperature of $CaCO_3$ (about 900°C under 1 bar of CO_2), less than 20% of the $CaCO_3$ in the limestone can be converted to CaS compared to 100% for dolomite. For the dolomitic limestone, all of the calcium atoms associated with the dolomite regions can be converted to CaS whereas only 20% of those associated with the limestone regions can be converted, yielding a maximum overall conversion of about 40%. Limestone is thus the preferred sorbent for coal-gas desulfurization, except at low temperatures (*i.e.*, below the temperature of calcination of $CaCO_3$) where only dolomites can be used effectively.

Kinetics of the reaction between H_2S and non-calcined limestone

In about 160 experiments with +6 mesh (1 to 2 mm diameter) batches of limestone, samples were exposed to an atmosphere of CO_2 (87-88%), H_2 (1-2%), CO (4-5%), H_2O (4-5%) and H_2S (0.5-1.85%) for various temperatures (570-860°C) and durations (5 to 240 min.)

(Fenouil and Lynn, 1995b). Limestone sulfidation was followed quantitatively as well as qualitatively to elucidate the reaction mechanism. The morphology of both the inside and the outside of reacted limestone samples was observed with a scanning electron microscope, and X-ray maps of the sulfur content of the reacted samples were generated. It was confirmed that up to the calcination temperature (about 870°C), the conversion of $CaCO_3$ to CaS stays below 10% when the stones are exposed to about 2% H_2S for up to four hours. It was also observed that the sulfur was homogeneously distributed throughout the samples, thus ruling out any pore diffusion limitation in the reaction kinetics.

It was shown that the kinetics of the chemical reaction between $CaCO_3$ and H_2S is the limiting step in the early stages of the sulfidation kinetics at low temperatures (up to about 670°C). At higher temperatures, a combination of recrystallization and sintering of the CaS product layer induces a sharp decrease in the reaction rate followed by another increase as the temperature is further increased (Fig. 1). The solid-state diffusion of the reacting gas (H_2S) through the sintered product layer of CaS becomes the limiting step in the reaction kinetics.

Using the Grain Model (Szekely *et al.*, 1976), we were able to describe this non-catalytic gas-solid reaction kinetics over the entire range of temperature (Fig. 1). It is important to note that this model contains essentially no adjustable parameters and that it is consistent with all the structural changes observed in the sulfided samples (Fenouil and Lynn, 1995b).

Kinetics of the reaction between H_2S and calcined limestone

Samples of the limestone particles described in the preceding section were then exposed to simulated coal-gases containing between 500 and 18,000 ppm of H_2S at temperatures ranging from 560 to 1100°C. Again, the formation of CaS was followed quantitatively as well as qualitatively to elucidate the reaction mechanism. The conversion of $CaCO_3$ to CaS was limited by the low permeability of the CaS layer to less than 20% for particles of this size when the partial pressure of CO_2 is sufficient to prevent calcination to CaO.

Limestone particles can be completely converted to CaS when the temperature is held above the calcination temperature of the calcium carbonate. The reaction actually takes place between CaO and H_2S following a shrinking-core mechanism with a very sharp interface between the unreacted CaO core and the CaS product layer (Fenouil and Lynn, 1995c). When the temperature is higher than 20 to 30°C above the calcination temperature of $CaCO_3$, the kinetics of limestone calcination (reaction 2) becomes faster than that of lime sulfidation (reaction 3) and does not interfere with the overall sulfidation kinetics. The kinetics of the sorption of H_2S by CaO is relatively insensitive to the reaction temperature (Fig. 2), and the reaction rate does not decrease significantly when the CaO is severely sintered for several hours at 1050°C prior to sulfidation. The CaS layer that forms on CaO appears to be much more permeable than that formed on $CaCO_3$, and conversion of millimeter-sized particles of CaO to CaS is complete in one to two hours if the H_2S concentration in the gas phase is maintained around 1%. Once CaO is formed, the reaction between CaO and H_2S is controlled by the diffusion of H_2S through the pores of the CaS product (Fig. 3). The effective diffusivity of H_2S through this layer is between 2.8×10^{-6} and 5.1×10^{-6} m^2/s. Using the random-pore model to estimate the effective diffusivity of H_2S in the solid, we found that the average pore radius in the CaS reacted layer was between 0.24 and 0.55 μm (leading to a Knudsen diffusivity of 1.4 to 3.2×10^{-4} m^2/s at 900°C).

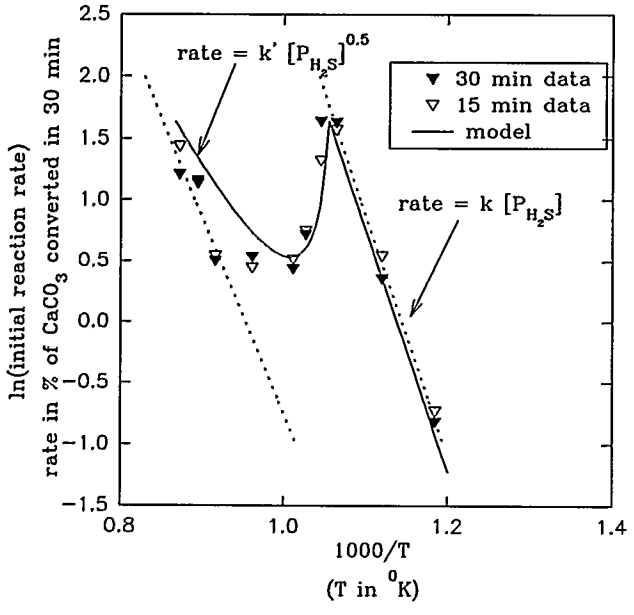

Fig. 1. *Change of Initial Reaction Rate Between $CaCO_3$ and H_2S with Temperature. Gas phase: CO_2(87.5%), CO(4.5%), H_2O(4.5%), H_2(1.7%), H_2S(1.8%).*

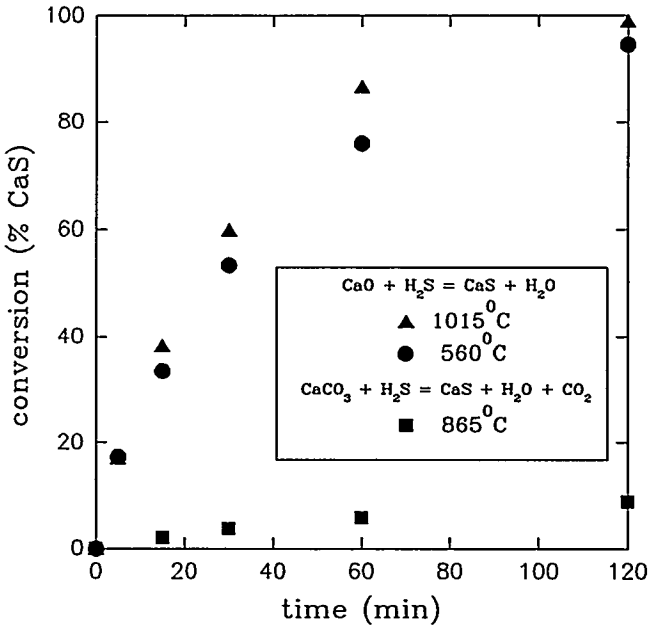

Fig. 2. *Effect of Temperature on Lime and Limestone Sulfidation (1.8% H_2S).*

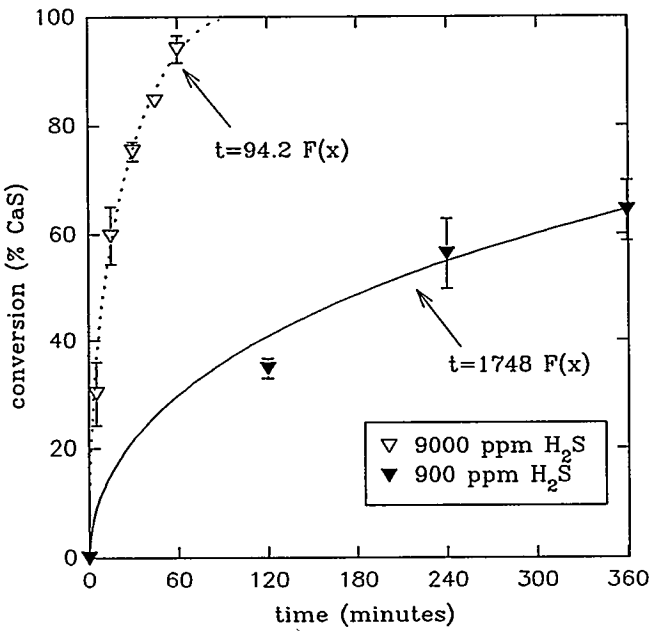

Fig. 3. *Conversion of CaO to CaS as a Function of Time (Single-Pellet Reactor). $F(X) = 1-3(1-X)^{2/3}+2(1-X)$*

Design of the coal-gas clean-up system

Design equations describing fixed beds as well as cocurrent and countercurrent moving beds of limestone particles sorbing H_2S (for plug-flow for gas and solid phase) have been developed and analytically solved for steady-state operation (or for constant-pattern breakthrough in the case of a fixed bed) using the Grain Model to describe the reaction kinetics:

$$t = (\tau_1 + \tau_2)\,[1 - 3\,(1-X)^{2/3} + 2\,(1-X)] = \tau_3 X + \tau_4\,[1 - (1-X)^{1/3}] \qquad (4)$$

where:

t = time,
X = fraction of solid converted to CaS,
τ_1 = characteristic diffusion time in the particle pores ($\rho_S R^2/(6D_e(C-C_{eq}))$),
τ_2 = characteristic diffusion time in the particle's grains ($\rho_S r^2/(6D_g(C-C_{eq}))$),
τ_3 = characteristic mass-transfer time ($\rho_S R/(3k_g(C-C_{eq}))$),
τ_4 = characteristic chemical reaction time ($\rho_S r/(k_s(C-C_{eq}))$),
k_g = mass-transfer coefficient in the gas film around the solid particle (m/s),
k_s = chemical reaction rate (m/s),
R = effective average radius of lime/limestone pellet (m),
r = average grain radius (m),
C = molar concentration of H_2S in the coal gas,
C_{eq} = equilibrium concentration of H_2S,
D_e = effective diffusivity of H_2S in the pores of the particle,
D_g = diffusivity of H_2S in the grains, and
ρ_S = molar density of the solid.

The concentration profile of H_2S and CaS along the bed length as well as the degree of utilization of the sorbent, the degree of removal of H_2S from the gas and the required bed total length can be expressed as a function of only five parameters: R, the radius of the limestone particles; y_{eq}, the thermodynamic equilibrium mole fraction of H_2S in the gas under bed conditions; $Sh' = 2(\tau_1+\tau_2)/\tau_3$, a modified Sherwood number (or Biot number); $Pe' = 6(\tau_1+\tau_2)/\tau_5$, a modified Péclet number (τ_5 is a characteristic flow time, equal to $(R(1-\varepsilon)\rho_S)/(u_G(C-C_{eq}))$ in the case of a fixed or moving bed, u_G being the superficial velocity of the gas); and $Da' = 6(\tau_1+\tau_2)/\tau_4$, a modified Damköhler number. The details of the models as well as its complete derivation can be found elsewhere (Fenouil, 1995).

Figure 4 provides an example of H_2S concentration profile as a function of the bed length for counter-current gas/solid flow in a moving bed (limestone particles of 2 mm diameter, 95% sorbent utilization, 98% sulfur removal (y_{out} = 200 ppm, y_{eq} = 180 ppm)). Using the kinetic data described in the preceding section and reasonable estimates of the operating conditions of a moving bed of limestone particles (*i.e.*, Pe' on the order of 1000, Sh' on the order of 200, Da' being extremely large), the total bed length is found to be of the order of 1 meter.

Conclusions

Limestone presents the advantage of being cheap, easily available and relatively safe to handle. It is also among the best in thermodynamic performance for H_2S removal from coal gas at and above 800°C, where zinc-based sorbents cannot be used. Furthermore, preliminary results suggest that calcium sulfide can be easily, and economically, regenerated to calcium carbonate with a low-temperature process still under development, and that the sulfur can subsequently be recovered as the element (Fenouil and Lynn, 1995d). For all these reasons, it appears to be the most suitable sorbent for high-temperature coal-gas desulfurization.

References

Fenouil LA. Kinetic and structural studies of the sulfidation of large particles of lime and limestone in coal gas. Ph.D. dissertation. University of California at Berkeley, 1995.

Fenouil LA, Lynn S. Comparison of calcium-based sorbents for coal gas

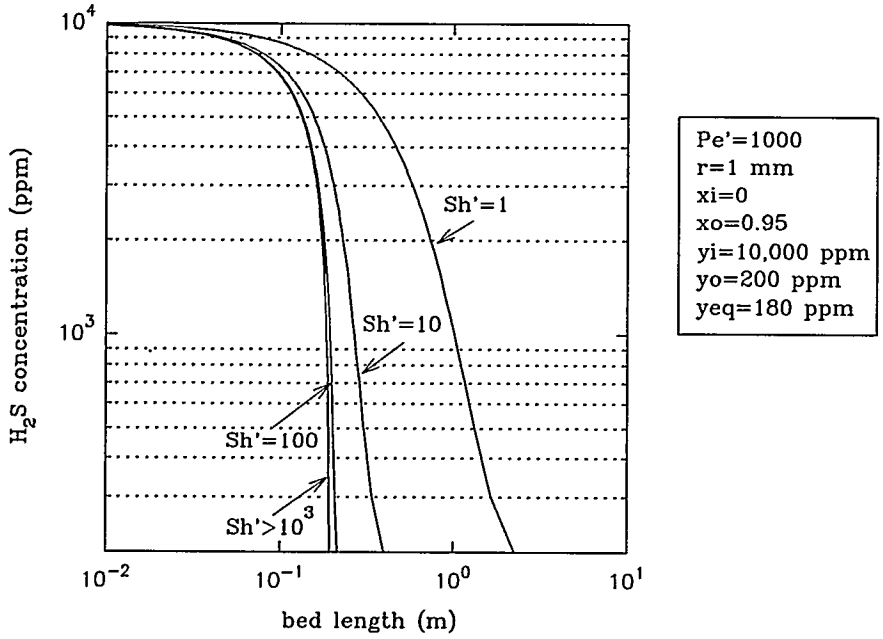

Fig. 4. *H_2S Concentration as a Function of Bed Length for Counter-Current Flow Configuration (Da' = ∞).*

desulfurization. Accepted for publication in *Ind. Eng. Chem. Res.*, 1995a.

Fenouil LA, Lynn S. Kinetics of the reaction between H_2S and non-calcined limestone under simulated coal gas. Accepted for publication in *Ind. Eng. Chem. Res.*, 1995b.

Fenouil LA, Lynn, S. Kinetics of the reaction between H_2S and calcined limestone under simulated coal gas. Accepted for publication in *Ind. Eng. Chem. Res.*, 1995c.

Fenouil LA, Lynn S. Kinetic and structural studies of calcium-based sorbents for high-temperature coal-gas desulfurization. Accepted for publication in *Fuel Science and Technology International*, 1995d.

Fenouil LA, Towler GP, Lynn S. Removal of H_2S from coal-gas using limestone: kinetic considerations. *Ind. Eng. Chem. Res.*, 1994; 33(2): 265-272.

Other Literature Cited

Szekely J, Evans JW, Sohn HY. *Gas solid reactions*, Academic Press, New York, 1976.

Separations by Reversible Chemical Complexation

C.J. King

Carboxylic acids, glycols and related polar organics are among the most attractive products that can be manufactured from biological raw materials by fermentation. Selective recovery of these products from fermentation media is difficult, because the solutions are dilute and complex. Separations of these substances from dilute aqueous solutions are also important for production of several large-volume petrochemicals, such as acetic acid and ethylene and propylene glycols, and for processing of numerous waste streams. Separations based upon reversible chemical complexation with organic agents have strong potential for processing of these streams, and are the focus of our research.

Recovery of Glycols by Reversible Complexation

Because of their low volatilities and high hydrophilicities, the separation of gycols from water solution poses a difficult, but important, problem. Following an investigation of recovery of cis-vicinal diols by reversible reaction with aldehydes to form dioxolanes, we have returned to investigation and development of ways of using reversible complexation with organoboronates for glycol recovery. Boronate anions form reversible cyclic complexes with cis-vicinal diols.

More precise measurements were made of the partition coefficient of propylene glycol from water into 2-ethylhexanol, the diluent used in our earlier research in this area. This refinement enabled better interpretation of our earlier data for extraction of propylene glycol by an Aliquat 336-nitrophenylboronate ion pair in 2-ethylhexanol diluent. We made further measurements, with more readily available phenylboronate replacing the nitrophenylboronate anion. Interestingly, these results display up to about 40% stoichiometric overloading, *i.e.*, up to 1.4 moles of propylene glycol chemically extracted per mole of phenylboronate.

We have used carbon dioxide as an agent to displace phenylboronate from the complexed ion pair, forming phenylboronic acid. Since glycols complex with only anionic boronates and not with boronic acids, this procedure releases the complexed glycol for back extraction into water as a concentrate. Heating and stripping the solution of the resultant Aliquat 336-bicarbonate ion pair releases the volatile CO_2, returning the phenylboronic acid to the anionic phenylboronate form and thereby readying the extractant for reuse. We have found loss of capacity of the ion-pair extractant upon regeneration and reuse. This appears to be due to thermal degradation, a phenomenon that we are investigating further.

We have also investigated implementation of boronate complexation by means of solid adsorbents. Amberlite IRA-910 (Rohm & Haas), a quaternary ammonium adsorbent, was paired with phenylboronate anion, but the resultant adsorbent showed a much lower complexation constant with propylene glycol. This apparently results from the complexation occurring in an aqueous environment, rather than in an organic environment as is the case for extraction. Another approach investigated was the use of specialty solid sorbents where the boronate functionality is built into the solid structure. One such adsorbent displayed very low capacity for propylene glycol, perhaps again because of the aqueous environment.

Production of Calcium Magnesium Acetate

Calcium magnesium acetate (CMA) is an environmentally benign de-icer for highways, runways, etc., and is receiving considerable attention. If fermentation is the source of the acetic acid for CMA manufacture, then reversibly complexing extraction or adsorption can be used to recover the acetate anion selectively from the fermentation medium. Fermentations to produce acetic acid function best at pH 5.5-6.0, which is substantially above the pK_a of acetic acid, meaning that the product exists as acetate anion, rather than as undissociated acetic acid. Nonetheless, an extractant or adsorbent of appropriate basicity can then be contacted with an aqueous slurry of dolomitic lime (CaO/MgO) to make a concentrate of CMA, which can then be spray dried to provide the solid CMA product.

We investigated a number of adsorbents and extractant/diluent combinations in order to interpret the relevant chemistry and to identify those that would give the best overall performance. Amberlite IRA-35 (Rohm & Haas Corp.), a resin with secondary amine groups, sustains capacity to pH 6.0 and above, and yet is regenerable with an aqueous slurry of dolomitic lime. Among extractants, Amberlite LA-2 (Rohm & Haas Corp.) with a n-octanol as diluent sustains capacity to pH 6.0 and is similarly regenerable.

Previous research elsewhere, which had not been sensitive to the pH issue, identified trioctylphosphine oxide (TOPO) as a desirable extractant. However, TOPO is not sufficiently basic to sustain capacity in the pH range of interest for fermentation.

Recovery of Carboxylic Acids at $pH > pK_a$

We have been investigating methods for regeneration of basic solid sorbents and liquid extractants that are effective at pH above the pK_a of the carboxylic acid, which is the condition usually encountered in fermentations to produce carboxylic acids. (Citric acid is a notable exception.) In our earlier research we used leaching or back-extraction with aqueous trimethylamine (TMA), followed by thermal decomposition of the resultant trimethylammonium carboxylate. This method works successfully except for difficulty in removing the last TMA from a highly soluble, self-associating acid, such as lactic acid. We are now seeking alternatives to TMA, which is itself a rather unpleasant substance.

We examined distillative change of the diluent as an approach for regenerating basic sorbents and extractants that are effective for recovering carboxylic acids at pH above the pK_a of the acid. We have used an extractant composed of Alamine 336 (a tertiary amine, Henkel Corp.) in a diluent containing both n-octanol and dodecane. The idea is that octanol would be distilled from the diluent after extraction and before regeneration, which would occur by back-extraction into water. Then the octanol would be added back to the diluent as the regenerated extractant is recycled for the primary extraction. Since octanol solvates the acid-base complex much better than does the alkane, the equilibrium organic/aqueous distribution ratio for the forward extraction should be much greater than that for the back-extraction. We have utilized both acetic and lactic acids, while recognizing that the volatility of acetic acid would preclude use of such a process for it. Results show that at a given temperature the acid-base complexation constant changes by a factor of 50 to 100 between a diluent containing 5% dodecane and 95% octanol, and one containing 95% dodecane and 5% octanol. A swing of temperature from 25°C to 60°C can provide another factor of 4 change. Further, removal of that much octanol by distillation greatly enhances the phase ratio for back-extraction into water.

Recovery of Sugars by Adsorption onto Activated Carbons

Activated carbons adsorb significant amounts of sugars. Since most sugars exhibit negative deviations from ideality in aqueous solution, the positive adsorption must result from preferential chemical interactions. We carried out experiments adsorbing glucose from aqueous solution onto fifteen different commercial carbons at 25°C, with the aims of defining the uptake capacities, identifying and rationalizing the differences among carbons, and determining the reversibility of adsorption. Uptake capacities in equilibrium with 1% (w/w) glucose solution were in the range 0.015 to 0.20 g glucose/g carbon and varied considerably from carbon to carbon. Four of the carbons with higher capacities were tested for reversibility of adsorption. Within experimental precision, adsorption onto Filtrasorb 100 and 400 (Calgon Corp.) and Witcarb 950 (Witco Chemical Co.) were fully reversible, while adsorption onto RO 0.8 (Norit Co.) showed some apparent irreversibilty. The relationship between capacity and properties of the carbons is not apparent, and we are therefore pursuing studies in that area. There are many large and important applications for which a method of recovery of sugars from dilute aqueous solution would be valuable. In addition, if activated carbon is to be used for recovery of fermentation products, one would seek in that case to minimize simultaneous uptake of sugar substrates.

References

Broekhuis RR, Lynn S, King CJ. Recovery of Propylene Glycol from Dilute Aqueous Solutions via Reversible Reaction with Aldehydes. Lawrence Berkeley Laboratory Report No. LBL-35155, December 1993.

Lee JH, Van Brunt V, King CJ. Water-enhanced solvation of organic solutes in ketone and ester solvents. *Ind. Eng. Chem. Research* 1994; 31: 1373-1379.

Randel LA, Chow TK, King CJ. Ion-pair extraction of multi-OH compounds by complexation with organoboronate. *Solvent Extr. & Ion Exch.* 1994; 1: 765-778.

High Resolution X-ray Fluorescence Spectroscopy

S.P. Cramer, M.M. Grush, J.A. Moore, C.R. Randall, and X. Wang

X-ray absorption spectroscopy (XAS), in particular Extended X-ray Absorption Fine Structure (EXAFS), has been very useful in determining the coordination chemistry of metal centers in a wide variety of materials. However, one of the limitations of conventional XAS is that the contributions from all of the species of a given element are averaged together in the spectrum. The signals from different species are usually unresolved, making interpretation of individual site structures difficult or impossible. Since many important metalloenzymes contain two or more atoms of a particular transition element, often in different oxidation states and chemical environments, the ability to characterize individual sites would be an important development.

Small but resolvable shifts occur in the fluorescence emission from metals in different oxidation states or spin states. For example, it has been found that the

$K_ß$ features shift significantly between Mn(II) and Mn(III), and somewhat less between Mn(III) and Mn(IV). By combining high-resolution fluorescence detection with high-resolution absorption measurements, two distinct advantages are gained. First, the measurements can be made selectively for a particular oxidation state or spin state by choosing the appropriate region in an emission spectrum. Second, the absorption spectra that can be obtained are sharper than normal K-edge spectra. With the ability to study elements with particular site symmetries or oxidation states in isolation, site-selective spectroscopy could be a powerful new probe of complex systems.

Recently, a spherically bent Si(440) spectrograph was used to record the high-resolution x-ray fluorescence spectra of a series of Mn compounds. The $Kß_{1,3}$ feature (stronger main peak) shifts to lower energy with increasing oxidation state, while the Kß' feature (weaker satellite) shifts to higher energy and virtually disappears for low-spin Mn(III) and all Mn(IV) compounds. We developed the first spectrograph for Fe Kß fluorescence emission using a spherically bent Ge(620) crystal, and recorded spin-dependent X-ray Absorption Near-Edge Spectroscopy (XANES) spectra. The 1s→3d transition disappears when the Kß' emission is monitored.

We recently obtained high-resolution Kß fluorescence spectra of a $Mn(II,III_2)$ trinuclear complex, $Mn_3O(O_2CC_6H_5)_6(py)_2(H_2O)$ (Figure, left). For comparison, the emission spectra of MnF_2 and $Mn(OAc)_3{\cdot}2H_2O$ are shown. They explain our rationale in selecting the energies to monitor in recording EXAFS spectra. Preliminary analysis shows marked differences between the EXAFS spectra (Figure, right) obtained with monitoring the Kß emission at 6492.6 eV (Mn^{2+} side) and at 6488.9 eV (Mn^{3+} side).

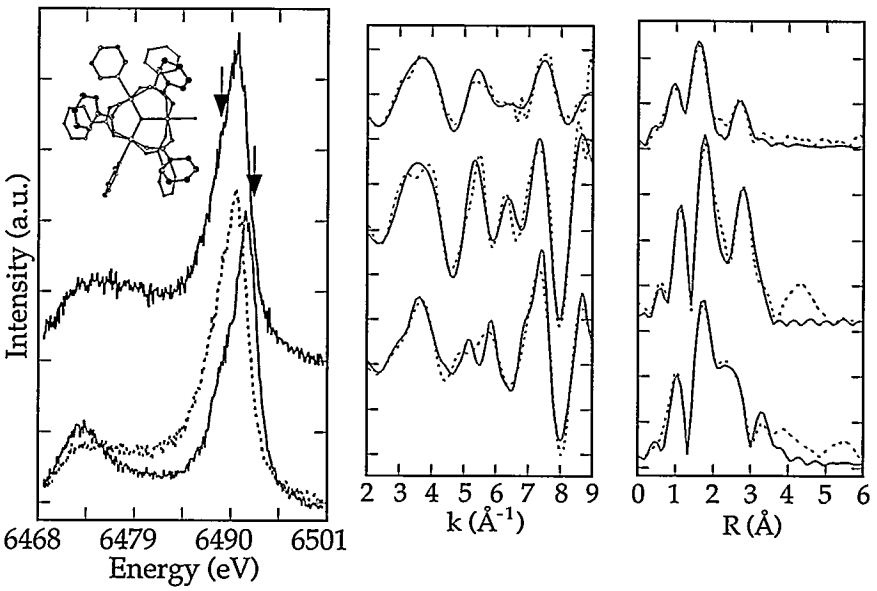

Figure. *Left: Kß emission spectra of $Mn_3O(O_2CC_6H_5)_6(py)_2(H_2O)$ (top, structure in inset), $Mn(OAc)_3{\cdot}2H_2O$ (dotted line) and MnF_2 (bottom, solid line). Middle: Preliminary EXAFS spectra of $Mn_3O(O_2CC_6H_5)_6(py)_2(H_2O)$: transmission (top), site-selective Kß fluorescence spectrum recorded with monitoring at 6492.6 eV (middle) and at 6488.9 eV (bottom). Right: Fourier transforms of EXAFS spectra in middle figure.*

References

Peng G, de Groot FMF, Hämäläinen K, Moore JA, Wang X, Grush MM, Hastings JB, Siddons DP, Armstrong WH, Mullins OC, Cramer SP. *J. Am. Chem. Soc.* 1994; 116: 2914.

Hämäläinen K, Kao C-C, Hastings JB, Siddons DP, Berman LE, Stojanoff V, Cramer SP. *Phys. Rev. B* 1992; 46: 14274.

Peng G, Wang X, Randall CR, Moore JA, Cramer SP. *Appl. Phys. Lett.*, 1994; 65: 2527.

Bioorganometallic Chemistry: The Reactions of (η^5-Pentamethylcyclopentadienyl)rhodium Aqua Complexes with Nucleobases, Nucleosides, Nucleotides, and Oligonucleotides

R.H. Fish, H. Chen, M.M. Olmstead, M.S. Eisen†, D.P. Smith, M.F. Maestre*

Bioorganometallic chemistry is a relatively new aspect of metal-carbon bond compound reactivity that is focused on the reactions of organometallic aqua complexes with biological substrates in aqueous solution. We have been studying the reactions of nucleobases, nucleosides, nucleotides, and oligonucleotides in aqueous solution with Cp*Rh aqua complexes, as a function of pH. In this FY, we demonstrated the rich and diverse structural chemistry uncovered via reaction of $[Cp^*Rh(H_2O)_2(OTf)_2]_x$ with 9-methyladenine, 1-methylcytosine, 9-ethylguanine, 9-methylhypoxanthine, 9-ethylhypoxanthine, adenosine, guanosine, adenosine and methyl-5'-adenosine monophosphates, and the oligos, dA_{2-4} and dA_{12}, at various pH values.

References

Fish RH, Smith DP, Chen H, Maestre MF, Olmstead MM, Eisen MS, Haskel A. Bioorganometallic chemistry: The reactions of a (η^5-pentamethylcyclopentadienyl)rhodium aqua complex with nucleobases, nucleosides, nucleotides, and oligonucleotides. In: NATO Series on

*Department of Chemistry, University of California, Davis, CA 95616

†Department of Chemistry, Technion-Israel Institute of Technology, Haifa, 32000, Israel

Advanced Technology 1995 (in press J. Am. Chem. Soc.).

Chen H, Maestre MF, Fish RH. Bioorganometallic chemistry. 5. Molecular recognition of aromatic amino acid guests by Cp*Rh-nucleobase/nucleoside/nucleotide cyclic trimer hosts in aqueous solution. (*J. Am. Chem. Soc.* in press).

Eisen MS, Haskel A, Chen H, Olmstead MM, Smith DP, Maestre MF, Fish RH. Aqueous organometallic chemistry: Structure and dynamics in the formation of (η^5-pentamethylcyclopentadienyl)rhodium aqua complexes as a function of pH. (*Organometallics* in press 1995).

Chen H, Olmstead MM, Smith DP, Maestre MF, Fish RH. The pH dependent synthesis and structural studies of monomer, dimer, and cyclic trimer complexes from the reactions of 9-methylhypoxanthine/9-ethylhypoxanthine nucleobases with (η^5-pentamethylcyclopentadienyl) rhodium aqua complexes (submitted for publication).

Removal and Recovery of Toxic Metal Ions from Aqueous Waste Streams by Utilization of Polymer Pendant Ligands

R.H. Fish, S.-P. Huang, W. Li, J. Devenyi, and R. Albright

The purpose of this project is to investigate the use of polymer pendant ligand technology for the removal and recovery of economical and toxic metal ions from DOE waste streams. Polymer pendant ligands are organic ligands, bound to cross-linked, modified divinylbenzene-polystyrene beads, that are capable of selectively complexing metal ions. The metal ion removal step usually occurs through a complexation or ion exchange phenomena, and thus, recovery of the metal ions and reuse of the beads is readily accomplished.

The research objectives, which we have achieved this fiscal year, includes synthesis of selective polymer pendant ligands for removal and recovery of the metal ions of interest to the Efficient Separations and Processing (ESP) program goals, determination of rates of both removal and recovery of these metal ions, and gaining industrial partners for implementation of the polymer pendant ligand technology we have generated. The studies have initially focused on the waste waters of the Berkeley Pit (~pH = 2.5) located in Butte, Montana, with emphasis on the following metal ions, Fe^{3+}, Al^{3+}, Cr^{3+}, Cu^{2+}, Zn^{2+}, Mn^{2+}, Mg^{2+}, Ni^{2+}, and Ag^{+}. Since Fe^{3+} was dominant in the Berkeley Pit waste waters, we placed special attention on devising Fe^{3+} selective polymer pendant ligands in order to be able to remove and recover the other economically important metal ions such as Cu^{2+}, Zn^{2+}, Mn^{2+}, Mg^{2+}, and Al^{3+}.

The removal and recovery of metal ions from aqueous waste streams is an area that will demand a considerable amount of attention for technology development. In addition to developing a wide range of technologies for specific metal ion removal and recovery applications, the tremendous advantage in having a generic based technology is that it can accommodate a wide range of applications with regard to metal ion and waste stream to be treated. Clearly, the cost effectiveness of the polymer pendant ligand technology would make it an excellent alternative to cumbersome precipitation techniques.

Accomplishments

The first priority for this task was to develop selective polymer pendant ligands for iron (Fe^{3+}) removal and recovery and our experimental studies at LBL have successfully accomplished this aspect. The polymer pendant catechol ligand derivatives, sulfonated catechol, sulfonated 2-6-LICAMS, and sulfonated 3,3-LICAMS, were ideal biomimetic candidates for an Fe^{3+} selective polymer pendant ligand, since they are structurally similar to biological ligands that selectively sequester Fe^{3+} (See Structures for CATS, 2-6-LICAMS, and 3,3-LICAMS).

We have, therefore, been able to

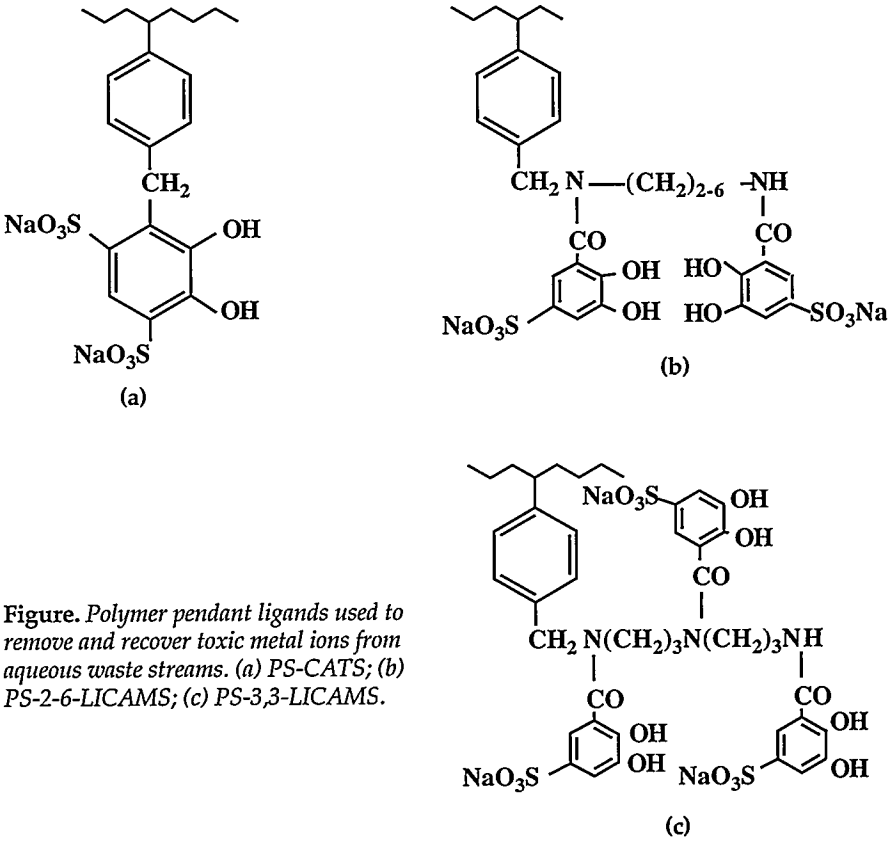

Figure. *Polymer pendant ligands used to remove and recover toxic metal ions from aqueous waste streams. (a) PS-CATS; (b) PS-2-6-LICAMS; (c) PS-3,3-LICAMS.*

synthesize and evaluate the Fe^{3+} selectivity for the above-designated polymer pendant ligands. From pH values of 0.5 to 2.5, we have found the following order for removal of Fe^{3+} from aqueous solution: **3,3-LICAMS >>>> CATS >> 2-6-LICAMS** with high capacities (0.8 to 1 mmol/g beads) and excellent removal kinetic rates ($2\text{-}4\times10^{-4}$/sec). Recovery of Fe^{3+} from the beads and then reuse of the beads was readily accomplished using a 2N H_2SO_4 solution. These important Fe^{3+} results have allowed us to be able to remove the divalent metal ions such as Cu^{2+}, Zn^{2+}, Mn^{2+}, Mg^{2+}, and Ni^{2+} with the **2-6-LICAMS** polymer pendant ligands; unfortunately, without selectivity to any particular divalent metal ion.

In addition, the above designated polymer pendant ligands have been found to also have utility in other DOE remediation problems, for example, selectively removing several radionuclides, Cs^{+} and Sr^{2+}, and environmentally important metal ions such as Hg^{2+} and Pb^{2+} from aqueous solutions. As well, we will also present data on several new polymer pendant ligands that are highly selective to Ag^{+} and Al^{3+}; both of high economic value in any resource recovery process to be designed for remediation of the Berkeley Pit. Finally, the synthesis of new metal molecular recognition polymers will be described that will introduce a new concept for selective removal and recovery of metal ions from aqueous waste solutions.

References

Huang S-P, Li W, Franz K, Albright R, Fish RH. Polymer pendant ligand chemistry. 3. A biomimetic approach to metal ion removal and recovery from aqueous solutions with polymer-supported sulfonated catechol and linear catechol amide ligands. (submitted to *Inorg. Chem.*, 1994)

Huang S-P, Franz K, Olmstead MM, Fish RH. Synthetic and structural studies of a linear bis-catechol amide, N, N'-bis(2,3-dihydroxybenzoyl)-1,7-diazaheptane (5-LICAM), and its complexes with Ni^{2+} and Co^{2+}: Utilization of a polymer supported, sulfonated analogue, 5-LICAMS, as a biomimetic ligand for divalent metal ion removal from aqueous solution. (submitted to Inorg. Chem., 1994)

Fish RH. "Polymer Pendant Ligand Chemistry." Presentation given at the 207th National Meeting, American Chemical Society, March 13-17, 1994, San Diego, CA, I&EC Division, Abstract 218.

Fish RH. "Polymer Pendant Ligand Chemistry." Presentation given at Federal Environmental Restoration III, Hazardous Waste Symposium, April 27-29, 1994, New Orleans, LA.

Fish RH. "Polymer Pendant Ligand Chemistry." Presentation given at the International Symposium on Polymer Supported Reactions in Organic Chemistry, June 19-23,1994, Venice, Italy.

Fish RH. Sulfonated catechol and linear catechol amide polymer pendant ligands for removal and recovery of metal ions from aqueous waste streams (patent application in preparation by the LBL/DOE patent department); 1994. (Also published as DOE 5-81, 626 (RL-12749) 2/17/95).

Mechanistic Aspects of the Oxidation of Alcohols with MMO Biomimics in Aqueous Solution

R.H. Fish, A. Rabion, R.M. Buchanan, S. Chen,* J. Wang, and J.-L. Seris†*

The unique ability of water soluble methane monooxygenase enzymes (MMO) to oxidize a broad range of hydrocarbons has led to several environmental applications for the use of methanotrophic bacteria, including, bioremediation of land contaminated by oil spills, and the oxidative removal of trichloroethylene from drinking water. Therefore, the utilization of biomimics of MMO in aqueous solution for the oxidation of water soluble substrates, such as alcohols, would be of interest from a mechanistic focus; previous MMO biomimetic oxidation studies have all been performed in organic solvents.

In this fiscal year, we studied the mechanisms involved in the oxidation of two water soluble substrates, cyclohexanol and benzyl alcohol, using several LFeOFeL complexes as catalysts with TBHP as oxidant in aqueous solution. Initial studies, on the mode of TBHP O-O bond scission, show dramatic effects of water on the mechanism of cleavage, and provide strong evidence for a homolytic scission of the peroxide bond (in acetonitrile the O-O bond scission mainly occurs *via* a heterolytic pathway to give Fe=O and t-BuOH) to provide t-BuO· radicals. Thus, the t-BuO· radicals appear to be mainly responsible for the conversion of alcohol to ketone, not Fe=O complexes.

Reference

Buchanan RM, Chen S, Richardson JF, Bressan M, Forti L, Fish RH. Biomimetic oxidation studies. 8. The structure of a new MMO active site model, $[Fe_2O(H_2O)_2(tris((1\text{-methylimidazol-}2\text{-yl})methyl)amine)_2]^{4+}$, and the role of the aqua ligand in alkane functionalization reactions. *Inorg. Chem.* 1994; 33:3208.

*Department of Chemistry, University of Louisville, Louisville, KY 40292
†Groupement de recherche de Lacq, BP 34, 64170 Artix, France

Uranium-Dioxide Dissolution in Aqueous Solutions

R.E. Russo and J.D. Rudnicki

A sensitive photothermal deflection spectroscopic (PDS) technique has been developed for studying oxidation and dissolution of UO_2 in aqueous solutions. The PDS technique measures the optical absorption spectrum at the UO_2 surface and concentration gradients in the solution. The combination of these two measurements provides information that can be used to infer the UO_2 dissolution mechanisms. The optical absorption and concentration gradient data provide evidence for a recrystallization reaction followed by a slow chemical dissolution of the recrystallized species. Similar experiments performed on single-crystal UO_2 did not show the recrystallization process, supporting a hypothesis that recrystallization and dissolution are occurring primarily from grain boundaries and/or active sites. The number of grain boundaries in the crystalline material should be negligible compared to the sintered material, and provides a method for determining the role of grain boundaries on UO_2 dissolution.

The shape of our concentration-gradient deflection provides unique information that can be correlated with the electrochemical voltammograms. A main feature is a sudden jump in the concentration deflection when the oxidizing potential exceeds +300 mV. This deflection represents dissolution. Not only does the concentration deflection (dissolution) significantly increase at this potential, but it persists even under subsequent reducing conditions. There is no corresponding change in the electrochemical current-potential curves to explain the persistent deflection.

A candidate mechanism to describe these measurements is recrystallization of the surface at selected sites. Up to $UO_{2.33}$ the crystal lattice is stable in the face-centered cubic structure. Under the dynamic conditions of a potential sweep the surface composition may reach $UO_{2.33}$ around -300 mV. At some sites, perhaps located in the grain boundaries, recrystallization begins and dissolution becomes extensive because $UO_{2.33}$ is the limiting stoichiometry for which the fluorite lattice is stable. Because oxidative dissolution is occurring at potentials <300 mV, the most likely product of this recrystallization/reprecipitation process is $UO_3 \cdot 2\,H_20$. Recrystallization of the surface to $UO_{2.67}$ is also possible. The dissolution of $UO_3 \cdot 2\,H_20$ would be a chemical, not electrochemical, process consistent with our measurements. This recrystallization process appears to be confined to grain boundaries. To test this hypothesis, we performed similar experiments on the crystalline sample of UO_2. The crystalline material does not show the jumps in the concentration gradient, although the electrochemistry is similar to that of the sintered material. A model has been developed that correlates our photothermal deflection measurements with a potential dissolution mechanism.

Reference

Rudnicki JD, Russo RE. Photothermal deflection spectroscopy investigations of uranium dioxide oxidation. *J. Electroanal. Chem.* 1994; 372: 63-74.

Fundamental Studies of Laser-Material Interactions

R.E. Russo, A. Fernandez, X.L. Mao, and M.A. Shannon

When a high-power pulsed laser beam is focused onto a solid surface, it can cause the removal of material by melting, vaporization, sublimation, and a number of non-linear processes. A generic term, laser ablation, is regularly used to identify the overall interaction. Laser ablation offers several attractive features for chemical analysis: direct analysis of conductive and non-conductive solid materials, localized microanalysis, and minimal sample preparation. Qualitative and semi-quantitative analysis of a wide variety solid samples has been demonstrated using laser ablation sampling with a separate atomization and/or excitation source. The goal of this research is to study the fundamental processes underlying the explosive laser ablation, laser material interaction for accurate and sensitive chemical analysis.

The high-power laser material interaction initiates a luminous plasma above the solid surface. Compositional analysis of the sample can be obtained directly by measuring the optical emission spectra of the laser-induced plasma (LIP). LIP emission spectra consist of neutral atom and ionic lines superimposed on a spectrally broad-band continuum of radiation. The characteristics of the plasma are dependent on the laser irradiance, target composition, atmospheric conditions, and time. The continuum plasma emission background results from free-free or free-bound transitions through electron-ion recombination (Inverse Brehmstraahlung).

Laser-induced plasmas from solid copper targets in argon at atmospheric pressure were characterized by measuring their emission spectra and excitation temperature spatial profiles as a function of laser power density. The effect of converting integrated emission line intensities to excitation temperature during plasma expansion was studied, and a shock-wave model was used to demonstrate that the position of maximum emission intensity does not occur at the position of maximum temperature, rather it depends on the heat and mass transfer in the plasma. Relationships among plasma velocity, spatial position, and integration time to the measured emission intensity and temperature profiles were studied.

Spatially resolved, time-integrated Cu emission spectra from the laser-induced plasma, obtained using a 100-mm laser-beam spot size and 4.93 GW/cm^2 power density are shown (Figure 1). Cu emission lines at 510.55, 515.32, 521.82 and 529.25 nm are observed. Cu ion emission lines were not observed, only neutral emission lines. From the data in Figure 1, the copper lines extend about 3 mm above the metal surface, with the peak emission intensity at approximately 1.5 mm from the surface. The ratio of line emission intensity can be used to determine the excitation temperature of the plasma at each axial location. The axial intensity distribution is primarily dependent on the power density of the laser, which can complicate analytical utility. The normalized spatial distribution of

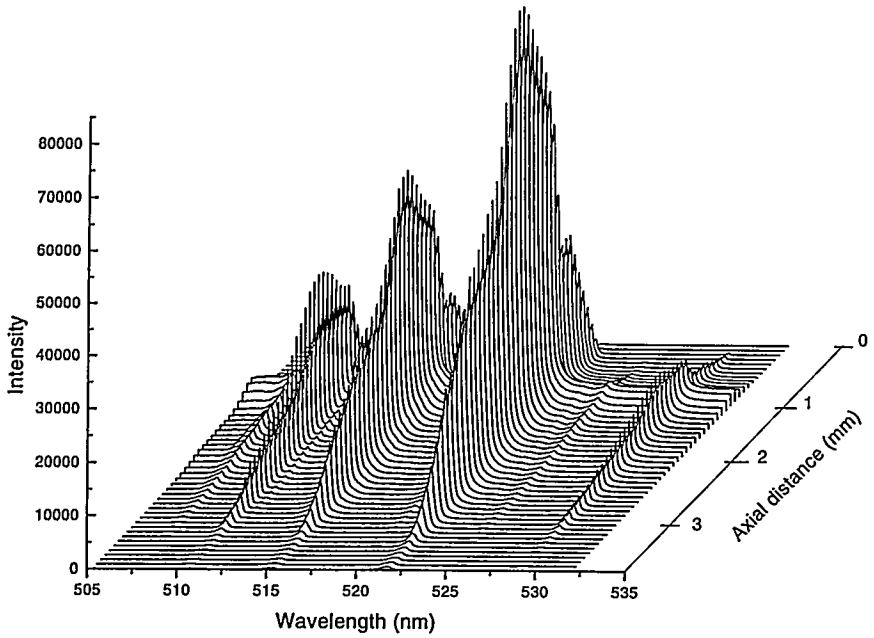

Figure 1. *Integrated Cu emission intensity versus axial position in the laser-induced plasma with power density of 4.93 GW/cm².*

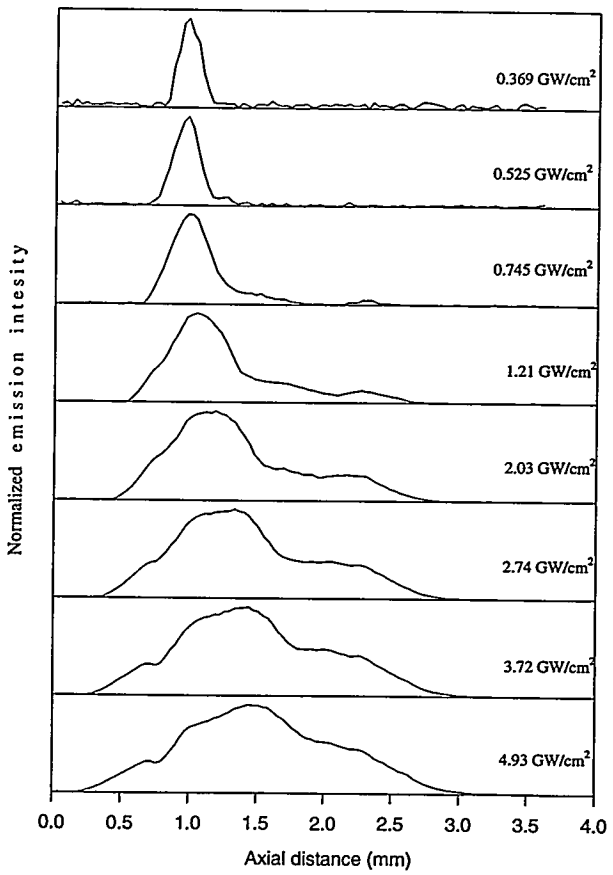

Figure 2. *Normalized axial spatial emission intensity versus power density.*

the 521.82 Cu emission intensity at laser power densities from 5 to 0.4 GW/cm² using a fixed 100-mm laser-beam spot size is shown (Figure 2). The spatial extent of the plasma diminishes as the power density decreases. The peak emission intensity is closer to the target surface at lower power densities. For low laser power densities, there is only one peak in the Cu emission intensity spatial profile compared to extensive shoulders at the higher laser power densities.

Temperature is an important property of an analytical excitation or atomization source and it needs to be known to understand vaporization, atomization, and excitation processes. In order to calculate the excitation temperature in the laser-induced plasma, the Boltzmann two-line method is used, based on the assumption that the Boltzmann distribution for excitation energy occurs in the second plasma region. The 521.82 nm and 510.55 nm atomic Cu emission lines are used to calculate the excitation temperatures reported in this work. For high incident laser power densities in which high LIP emission intensities are measured, the temperature can be calculated from 0.3 to 3 mm from the sample surface. In the case of low power density, the temperature can only be calculated from 0.7 to 1.8 mm from the target surface.

Excitation temperature spatial profiles calculated from the measured Cu emission profiles at two different power densities are shown (Figures 3, 4). For 0.525 GW/cm², the calculated excitation temperature varies from 11000 K to 6000 K and decreases with distance from the surface. At 4.93 GW/cm², the temperature is 12000 K at a height of 0.3 mm and then decreases to 7200 K at 2 mm. It then increases to about 8500 K at 2.5 mm and decreases again to 7500 K. The maximum in the temperature spatial profile does not overlap with maximum plasma emission intensity. The maximum temperature is always closest to the target surface before the emission intensity has peaked. To fully analyze the intensity and temperature spatial distributions requires a complete description of dynamic plasma expansion, excitation, and quenching which is outside the scope of this paper. However, by using a shock wave model, we demonstrate that the offset in these data is likely due to the measurement technique in which time-integrated emission intensity is measured during plasma expansion.

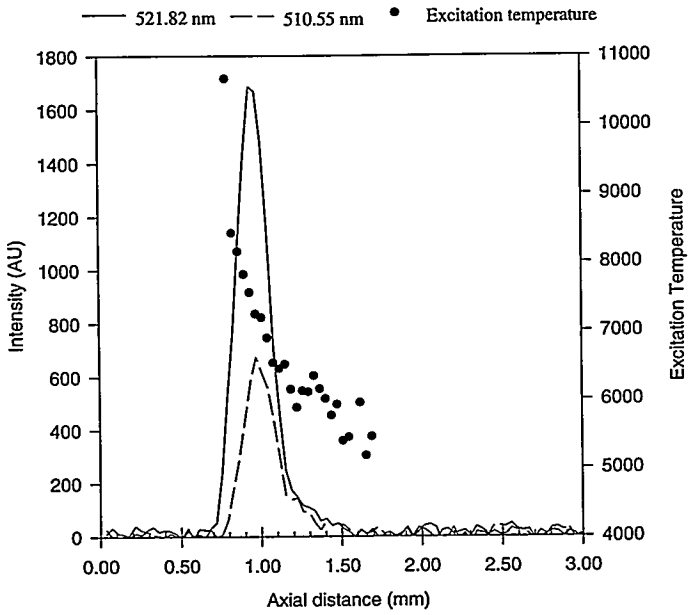

Figure 3. *Measured Cu(I) integrated emission intensities (solid and dashed lines) and calculated excitation temperature (dotted line) versus axial position in the laser induced plasma with a power density of 4.93 GW/cm².*

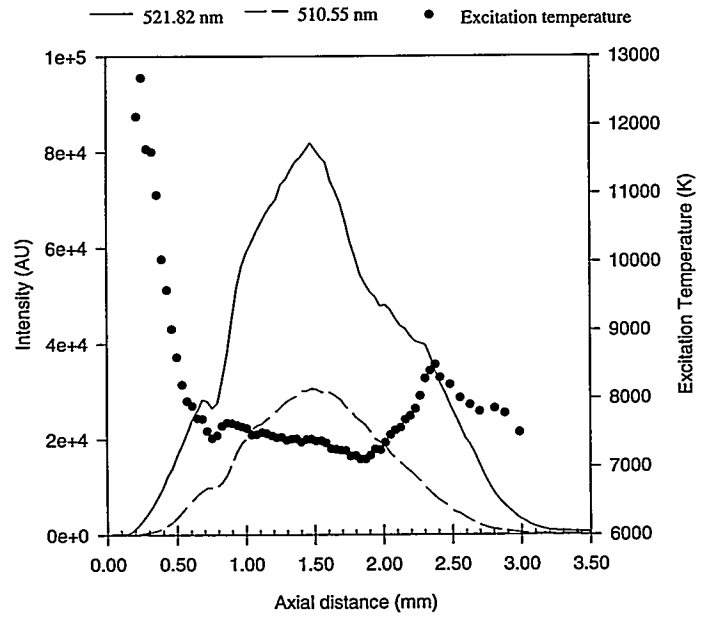

Figure 4. *Measured Cu(I) integrated emission intensity and calculated excitation temperature versus axial position in the laser induced plasma with a power density of 4.93 GW/cm².*

References

Xu X, Grigoropoulos CP, Russo RE. Transient temperature measurement during pulsed excimer laser heating of thin semiconductor films. (submitted to *J. Heat & Mass Transfer*)

Xu X, Grigorpoulos GP, Russo RE. Heat transfer in excimer laser melting of thin polysilicon layers. (submitted to *J. Heat & Mass Transfer*)

Shannon MA, Rubinsky B, Russo RE. Detecting laser induced phase change at the surface of solids via latent heat of melting with a photothermal deflection technique. *J. Appl. Phys.* 1994: 75: 1473-1485.

Xu X, Grigoropoulos CP, Russo RE. Measurement of solid/liquid interface temperature during pulsed excimer laser melting of polycrystalline silicon films. *Appl. Phys. Lett.* 1994; 65, 1745-1747.

Russo RE, Chan W-T, Bryant MF, Kinard WF. Laser ablation sampling with inductively coupled plasma atomic emission spectrometry for the analysis of prototypic glasses. (accepted by *J. Analytical Atomic Spectrometry*, November 1994)

Mao XL, Shannon MA, Fernandez AJ, Russo RE. Temperature and emission spatial profiles of laser-induced plasmas using ablation of solid samples. (submitted to *Applied Spectroscopy*, November 1994)

Qui TQ, Tien CL, Shannon MA, Russo RE. Thermal and mechanical response of gold films during nanosecond laser pulse heating, *J. Experimental Heat Transfer* 1995; 7: 175-188.

Material Applications

Optical Properties of the Ocean

A.J. Hunt, D. Miller, R. Garcia, M. Hayes, M.S. Quinby-Hunt, F.G. Shaw, D.B. Shapiro

The microstructured materials group has been involved for a number of years in various aspects of research into the optical properties of the ocean. In FY 1994 the work continued in two main directions; field and laboratory studies of the scattering and polarization properties of sea ice, and research into light scattering from non-spherical microorganisms. The latter investigations were conducted in a collaboration with Tennessee State University and were focused on gaining a better understanding of light scattering from chiral (right- and left-handed) structures.

The research into non-spherical structures investigated the light scattering from cylinders, helices, and other non-spherical particles characteristic of ocean waters as well as other asymmetrical forms that have structures with sizes roughly equivalent to the wavelength of the probing light. Two chiral systems were studied; octopus sperm heads from *Eledone cirrhosa* and a plectonemic helix, characteristic of some types of DNA. The scattering from the octopus sperm was predicted using a theory based on the Born approximation and the results were compared with laboratory measurements. A model was developed to predict the soft x-ray scattering behavior of a plectonemic helix. Calculations based on this model demonstrated that the orientation of the chromophores within the helix could be determined from x-ray scattering measurements.

Sea ice is a complex, heterogeneous, birefringent, and highly-variable material that exhibits strong polarization-dependent scattering. Understanding the optical properties of sea ice will enhance the ability of remote-sensing techniques to monitor and analyze the pack ice by measuring the polarized light it scatters. A description of the angle-dependent scattering and polarization properties of sea ice has not existed in the literature. Such a description is essential for models of radiative transfer through the ice, is useful in studying the orientation of the ice crystallinity, and aids in interpreting satellite data on ice pack characteristics.

To study polarization properties of sea ice we designed, built, and deployed a bi-static *in-situ* nephelometer instrument specially tailored to sit on the sea ice to probe the polarization characteristics of the ice. The measurement technique was based on our laboratory mono-static polarization-modulation instrument. The instrument was developed and tested at LBL and deployed for two weeks at two different sites near Point Barrow in April 1994 off the north Alaska coast in the Chukchi and Beaufort Seas at about 72 ° North. In the bi-static instrument, a laser and detector are separately pointed into the ice and their intersection determines the measurement site and scattering angle. The results of these measurements revealed an orientation dependence of the polarized light scattered within the ice and demonstrated that the linear polarization of light can be maintained for passage up to 60 cm within the ice.

To study sea ice under more controlled conditions our polarization-modulated angle-scanning nephelometer was modified to make measurements on samples from sea ice cores in the laboratory. A sample stage was designed to cool the samples to the eutectic temperature of sea ice brine (-23° C). Light scattering is measured from small cylinders and slabs of ice to investigate several of the matrix elements believed to be most sensitive to ice characteristics such as bubble and brine pocket structure, crystal orientation, and temperature.

The laboratory and field results will enhance the understanding of the scattering and polarization properties of sea ice. The data from the *in situ* and laboratory measurements will be useful in modeling efforts to understand light propagation in sea ice. This understanding can be applied to the results of remote sensing techniques to provide important information regarding issues such as ice formation, ice thickness, melting, and effects on shipping, wildlife, and climate change.

References

Hull PG , Shaw FG, Quinby-Hunt MS, Shapiro DB, Hunt AJ, LeightonT. "Comparison of Analytical Calculations with Experimental measurements for Polarized Light Scattering by Micro-Organisms." In: J.S. Jaffe, ed. *Ocean Optics XII.* SPIE 1994; 2258: 613-622.

Miller D, Hunt AJ, Quinby-Hunt MS. "Polarization-Dependent Measurements of Sea Ice." In: J.S. Jaffe, ed. *Ocean Optics XII.* SPIE 2258, 908-919, 1994.

Quinby-Hunt MS, Miller D, Hull PG, Hunt AJ. "Predicting Polarization Properties of Marine Aerosols." In: J.S. Jaffe Ed. *Ocean Optics XII.* SPIE 1994; 2258: 735-746.

Shapiro DB, Hull PG, Shi Y, Quinby-Hunt MS, Maestre MF, Hearst JE. Toward a working theory of polarized light scattering from helices. *J. Chemical Physics* 1994;100: 146-157.

Shapiro DB, Maestre MF, McClainWM, Hull PG, Shi Y, Quinby-Hunt MS, Hearst JE, Hunt AJ. Determination of the average orientation of DNA packed in the octopus sperm *Eledone cirrhosa* using polarized light scattering. *Applied Optics* 1994; 33: 5733-5744, .

Shapiro DB, Quinby-Hunt MS, Hearst JE, Hull PG, Hunt AJ. Light scattering from marine dinoflagellates: Single particle systems and ensembles. (submitted to *J. Geophysical Research*).

Shapiro DB, Hull PG, Hunt AJ, Hearst JE. Calculations of the mueller scattering matrix for a DNA plectonemic helix. *J. Chemical Physics* 1994;101: 4214-4222.

Nanocomposite Aerogel Materials

A.J. Hunt, M. Ayers, G. Barrio, W. Cao, L. Erskine, G. Kenney, D. Lee, M.S. Quinby-Hunt, X.Y. Song, P. Stevens, and S.Q. Zeng

Aerogels are porous, low density, nano-structured solids with many unusual properties including very low thermal conductivity, high porosity, transparency, high surface area, catalytic activity, and low sound velocity. Aerogels are prepared by solgel processing followed by supercritical evacuation of entrapped solvents. Current research involves developing new nanocomposite materials based on aerogel technology for a number of applications. Improving the thermal performance of aerogel, an important part of the research in recent years, has demonstrated that substantially improved thermal resistance can be achieved in aerogel insulation by adding finely dispersed carbon. New composite aerogel thermal insulation extends the range of applications to higher temperatures, provides a more compact insulation for space sensitive-applications, and lowers the cost of the aerogel by as much as 30%. Superinsulating aerogel can replace existing CFC-containing polyurethane insulation, reduce heat losses in hot and cold piping, insulate batteries in electric vehicles, and reduce energy losses in a variety of industrial applications. A Cooperative Research And Development Agreement (CRADA) was signed by LBL and Aerojet Corporation in 1994 to assist Aerojet with the commercial production of silica aerogel materials. In an extension of the aerogel research we have been exploring a much broader range of aerogel composite compositions. New composite materials have been prepared with unusual properties attributable to their very fine dimensions (such as quantum-size effects). These materials may be useful for new lightweight structural materials or used in magnetic cooling cycles, electroluminescent displays, and optical devices.

Thermal Insulation Research

Heat transfer in aerogel is more complex than in most other solids. Heat is transmitted by conduction through the solid phase, by the gas in the pores, and by radiation within the aerogel. Infrared radiation is responsible for half or more of the thermal conductivity in silica aerogel depending on its temperature and the pressure of the gas it contains. Reducing the infrared radiant heat transfer substantially improves the thermal performance of aerogel insulation. At elevated temperatures (200° to 500°C), the radiative component of heat transfer in aerogel becomes dominant and must be suppressed. The infrared radiation can be blocked by adding a finely dispersed material with a high absorption coefficient. We have developed a new method based on chemical vapor infiltration (CVI) to add carbon to aerogel that has many advantages over older methods in which particle are added in the sol or liquid stage. Nanostructured aerogel composites materials can be created by the process of using the catalytic decomposition of a gas inside the aerogel. This preparation method increases the strength of the aerogel and provides doping levels up to several times the original mass of silica.

To characterize the carbon-doped nano-composite materials prepared by the CVI method, infrared absorption and surface area were measured and High Resolution Electron Microscopy (HREM) was used to study the nanostructure. A Vacuum Insulation Conductivity Tester (VICTOR) was designed and built to measure the thermal conductivity of aerogel as a function of pressure and temperature. VICTOR was used to characterize doped and undoped aerogels. The best thermal performance of doped evacuated aerogels was about 4.5 mW/m/K (about ten times the thermal resistance of fiberglass insulation) and of non-evacuated doped aerogels was 13 mW/m/K. To analyze and predict the thermal performance of aerogel the heat transfer due to the radiation, conduction, and gas conductivity and their interaction inside aerogel was modeled. The objective is to predict the thermal conductivity as a function of temperature and gas pressure for various doped and undoped aerogels. The predicted effects of carbon doping on the thermal performance of aerogel are significant at higher temperatures and if borne out, opacified aerogel will be an outstanding insulating material for industrial applications for temperatures up to 500°C.

Development and Exploration of New Nano-Composite Materials

We are exploring a whole new family of unique nanoporous composite materials based on CVI of aerogel and other techniques. Nanophase composites were prepared with elemental silicon, iron, tungsten, and sulfur. Composites of silica aerogels and the oxides of iron, nickel, and copper were also synthesized using other techniques. Transmission electron microscopy was used extensively to characterize the nanostructure and crystallinity of the new composites. A wide variety of new composite materials can be produced using these methods. Such nanophase materials have potential applications in materials, magnetic cooling cycles, electroluminescent displays, and for transparent materials. Silicon-silica composites exhibit photoluminescence that our measurements confirm is due to quantum well confinement effects. These materials may be useful for electroluminescent display devices. The iron and iron oxide composites exhibit magnetic properties that appear useful for magnetic cooling cycles. A patent application covering the CVI-aerogel nanocomposite production process was filed in FY 1994.

References

Cao W, Hunt AJ. Thermal annealing of photoluminescent Si deposited on silica aerogels. *Solid State Commun.* 1994;91: 645-648.

Cao W, Hunt AJ. Photoluminescence of chemically vapor deposited Si on silica aerogels. *Applied Physics Letters* 1994; 642.

Cao W, Hunt AJ. Improving the visible transparency of silica aerogels. *J. Non-Crystalline Solids* 1994; 176, 18.

Cao W, Song XY, Hunt AJ. "Preparation and Characterization of Aerogel-Based Carbon Nanocomposites." In: C.L. Renschler, D.M. Cox, J.J. Pouch, and Y. Achiba, eds. *Novel Forms of Carbon II.* Pittsburgh: Materials Research Society, 1994: 87-92.

Cao W, Hunt AJ. Sol-gel processing using organo-functional silanes. *Proceedings of the Materials Research Society,* Spring 1994.

Hunt AJ, Ayers M. New route to aerogel composites using chemical vapor infiltration. *J. Non-Crystalline Solids* (accepted for publication).

Hunt AJ, Cao W. New routes to nanocomposite materials using aerogels. *Proceedings of the Materials Research Society,* Spring 1994.

Lee D, Stevens PC, Zeng SQ, Hunt AJ. Thermal characterization of carbon opacified silica aerogels. *J. Non-Crystalline Solids* (accepted for publication).

Zeng SQ, Hunt AJ, Cao WQ, Greif R. Pore size distribution and apparent gas thermal conductivity of silica aerogel. *J. Heat Transfer* 1994; 116: 756-759.

Zeng SQ, Hunt AJ, Greif R, Cao WQ. Approximate formulation for coupled conduction and radiation through a medium with arbitrary optical thickness. *J. of Heat Transfer* (in press).

Zeng SQ, Hunt AJ, Greif R, Cao WQ. Mean free path and apparent thermal conductivity of a gas in a porous medium. *J. Heat Transfer* (accepted for publication).

Zeng SQ, Hunt AJ, Greif R. Calculation of coupled conduction and radiation through an aerogel slab. *J. Heat Transfer* (accepted for publication).

Zeng SQ, Hunt AJ. Mean free path and apparent thermal conductivity of gas in aerogel. *J. Heat Transfer* (accepted for publication).

Zeng SQ, Hunt AJ, Greif R. Geometric structure and thermal conductivity of porous medium aerogel. *J. Heat Transfer* (accepted for publication).

Song XY, Cao W, Hunt AJ. "AEM and HREM Evaluation of Carbon Nanostructures in Silica Aerogels." In: C.L. Renschler, D.M. Cox, J.J. Pouch, and Y. Achiba, eds. *Novel Forms of Carbon II*. Pittsburgh: Materials Research Society, 1994: 269-274.

Song XY, Cao W, Ayers MR, Hunt AJ. Carbon nanostructures in silica aerogel composites. *Journal of Materials Research*, February 1995 .

Multilayer Thin-Film Structures Using Pulsed Laser Deposition

R.E. Russo, R.P. Reade, and P. Berdahl

High-temperature-superconductor (HTSC)-based multi-chip module (MCM) designs require several $YBa_2Cu_3O_7$-((YBCO) thin film layers in addition to low- and high-dielectric layers. The first layer is a superconducting ground plane, with several additional YBCO layers patterned as interconnects linking individual chips. Between the YBCO films, a relatively thick (~5 μm) low-dielectric layer is required. HTSC MCM designs require all layers to maintain an epitaxial relationship throughout the multilayer structure, and large area expensive single crystal substrates are not suitable. This requirement limits the choice of the dielectric material and the substrate, both must be lattice matched to the YBCO crystalline structure. It is difficult to find materials with a low dielectric constant, proper coefficient of thermal expansion, and the appropriate lattice constant for multilayer YBCO structures. Thus, it would be practical to eliminate the need for epitaxy throughout the layers of a HTSC MCM, or any HTSC multilayer structure.

Previously, we developed an ion-assisted pulsed laser deposition (IAPLD) process to deposit biaxially-aligned yttria-stabilized zirconia (YSZ) intermediate layers on polycrystalline and amorphous substrates. Using these layers, high critical current density (J_c) YBCO thin films were deposited on Haynes Alloy #230 (HA230), a polycrystalline Ni-based superalloy with a good coefficient of thermal expansion match to YBCO. High J_c is due to the in-plane alignment (or "biaxial alignment") induced by the ion-assisted process, which minimizes detrimental high-angle grain boundaries in the subsequently deposited YBCO. In the current work, we demonstrate the IAPLD technology for eliminating the epitaxial requirement throughout a HTSC multilayer structure. In particular, we demonstrate the use of amorphous dielectric layers and polycrystalline substrates in an HTSC MCM-type design.

Two different amorphous layer materials were used. The first is SiO_2, chosen due to its low dielectric constant (ε~3.8) and widespread use in microelectronics. SiO_2 is an excellent low-dielectric material but may be difficult to use with YBCO, as the coefficients of thermal expansion are significantly different for these materials, leading to the potential for cracking in the films. The second dielectric material is amorphous YSZ, chosen because its thermal expansion properties are similar to YBCO. The amorphous YSZ layer was chosen for demonstration purposes only, as the dielectric constant of YSZ (ε~25) is higher than acceptable for a HTSC MCM.

The SiO_2 layers were deposited on two different substrates. First, the SiO_2 was deposited in compression on the 1-mm-thick randomly-oriented polycrystalline HA230. Following the SiO_2, biaxially-aligned YSZ intermediate layers were deposited by IAPLD. Finally, YBCO was deposited *in situ* using the same conditions as in our previous work. The second "substrates" utilized for this study are YBCO/CeO_2/YSZ samples obtained commercially from Conductus, Inc. These samples consist of a 0.2-μm YBCO thin film deposited epitaxially on a two-inch single crystal YSZ substrate with a thin CeO_2 buffer layer. We fabricated an additional multilayer structure on top of these samples, consisting of thin YSZ intermediate layers, a thick low-dielectric layer, and an additional YBCO layer. Before deposition of the SiO_2 thick layer, the samples were diced into 1-cm squares, and an ~ 0.1-μm YSZ layer was deposited by pulsed-laser deposition at 200°C and 1.0 mtorr oxygen pressure to protect the YBCO film from chemical interaction with the SiO_2. After the SiO_2 deposition and prior to the deposition of the IAPLD YSZ and second YBCO layers, the structure is SiO_2/YSZ/YBCO/CeO_2/YSZ.

A YBCO/YSZ/SiO_2/HA230 multilayer structure was fabricated. Film thickness is approximately 0.4-μm YBCO, 0.2-μm YSZ, and 5-μm SiO_2. The film was highly c-axis oriented, as demonstrated by strong series of (00l) peaks in the x-ray diffraction. The superconducting transition temperature (T_c) of this film was ~87 K. A 50-μm-wide bridge was patterned for critical current density (J_c) measurements with and without a 0.4 T magnetic field. In the absence of magnetic field, the 77K J_c is 3×10^5 A/cm^2. At 73K in magnetic field, J_c is 7×10^3 and 2×10^3 A/cm^2 with field parallel and 45° to the film, respectively.

The requirements of epitaxy throughout the multilayer structure can be eliminated when the IAPLD technology is employed to deposit a thin oriented intermediate layer. In addition, these studies demonstrate that the primary parameter in designing multilayer structures is the coefficient of thermal expansion match among the materials.

References

Russo RE, Mao XL, Perry DL. Pulsed laser deposition of thin films. (accepted in *Chemtech*, September 1994)

Reade RP, Berdahl P, Schaper LW, Russo RE. Multilayer YBaCuO structures using ion-assisted intermediate layers. (submitted to *IEEE Transactions on Applied Superconductivity*, October 1994)

Reade RP, Berdahl P, Schaper LW, Russo RE. YBaCuO multilayer structures with amorphous dielectric layers for multichip modules using ion-assisted pulsed laser deposition. (submitted to *Applied Physics Letters*, December 1994)

Sponsors

Projects described in this report were supported by the following sources:

U.S. Department of Energy, Assistant Secretary for Energy Efficiency and Renewable Energy:

Office of Transportation Technologies, Electric and Hybrid Propulsion Division

Office of Industrial Technologies, Office of Industrial Processes

Office of Industrial Technologies, Advanced Industrial Concepts Division, Advanced Industrial Concepts Materials Program

U.S. Department of Energy, Assistant Secretary for Environmental Management & Restoration, Office of Technology Development, Office of Research and Development, Efficient Separations and Processing Integrated Program

U.S. Department of Energy, Office of Energy Research:

Office of Basic Energy Sciences, Chemical Sciences Division

Office of Health and Environmental Research, Medical Applications and Biophysical Research Division

Morgantown Energy Technology Center, Assistant Secretary for Fossil Energy, Office of Coal Utilization, Advanced Research and Technology Development, Division of Surface of Coal Gasification

Lawrence Livermore National Laboratory Contract No. W-7405-ENG-48

Office of Naval Research, Ocean, Atmosphere, and Space and Technology Department

United States Advanced Battery Consortium

Advanced Research Projects Agency (ARPA)

This support was provided through the U.S. Department of Energy under Contract No. DE-AC03-76SF00098.